energies

MDPI

Review

Research Progress on Flow Fields and Flow Channels of Proton Exchange Membrane Fuel Cells

Anbo Xu [1,2], Song Yang [1,2,*], Mengya Gao [1,2], Huili Dou [1,2], Jiahao Zhang [1,2], Yang Liu [3], Yunming Zhao [1,2], Jidong Li [1,2], Tingting Gao [1,2] and Haidong Bian [3]

[1] College of Automotive Engineering, Jilin University, Changchun 130022, China
[2] National Key Laboratory of Automotive Chassis Integration and Bionics, Jilin University, Changchun 130022, China
[3] Faw Jiefang Automotive Company, Changchun 130022, China
* Correspondence: yangsong1989@jlu.edu.cn

Abstract

Proton exchange membrane fuel cells (PEMFCs), characterized by high efficiency, zero carbon emissions, and low-temperature start-up capability, are among the most promising clean energy technologies. The design of flow channels and flow fields is critical for enhancing fuel cell power density, mitigating water flooding, and reducing costs. This paper systematically reviews the effects of key geometric factors in PEMFC flow fields and channels, including structural geometry, cross-sectional shape, and baffle design, on cell performance, with the aim of improving water management and enhancing PEMFC performance. Furthermore, the optimization of flow fields such as parallel, serpentine, and interdigitated configurations is reviewed as well. Particularly, the structural features and enhancement mechanisms of biomimetic and novel flow fields, as well as the advantages of three-dimensional flow fields in promoting mass transfer and improving water and thermal management, are discussed, thereby laying a foundation for the innovation and development of future high-performance proton exchange membrane fuel cells.

Keywords: proton exchange membrane fuel cells; flow channel structure; flow field design; three-dimensional flow field; water management; thermal management

Check for updates

Academic Editor: Francesco Lufrano

Received: 17 May 2026
Revised: 25 June 2026
Accepted: 27 June 2026
Published: 3 July 2026

Copyright: © 2026 by the authors. Licensee MDPI, Basel, Switzerland. This article is an open access article distributed under the terms and conditions of the Creative Commons Attribution (CC BY) license.

1. Introduction

Against the backdrop of the deep advancement of the global "dual carbon" strategy and the accelerated transformation of energy structures, addressing climate change and reducing dependence on fossil fuels has become a global consensus. Proton exchange membrane fuel cells (PEMFCs), with their outstanding advantages of zero carbon emissions, high energy conversion efficiency, and fast start-up capability, were regarded as highly promising clean energy solutions in fields such as transportation and distributed power generation [1–3]. Particularly in automotive applications, PEMFC technology was expected to fundamentally resolve the carbon emission issues of traditional internal combustion engines and the range and charging efficiency bottlenecks of battery electric vehicles [4,5]. Its core operating principle involved directly converting the chemical energy of hydrogen and oxygen into electrical energy through electrochemical reactions, with outputs of water. The electrochemical reactions are shown in Equations (1)–(3).

$$\text{Anode}: 2H_2 \rightarrow 4H^+ + 4e^- \quad (1)$$

$$\text{Cathode}: O_2 + 4H^+ + 4e^- \rightarrow 2H_2O \quad (2)$$

$$\text{Overall reaction}: 2H_2 + O_2 \rightarrow 2H_2O \quad (3)$$

In general, fuel cells can be categorized into six major types by fuel and electrolyte. They include polymer electrolyte membrane fuel cells (PEMFCs), alkaline fuel cells (AFCs), phosphoric acid fuel cells (PAFCs), molten carbonate fuel cells (MCFCs), solid oxide fuel cells (SOFCs), direct methanol fuel cells (DMFCs) and direct ethanol fuel cells (DEFCs). Unlike high-temperature solid oxide fuel cells, molten carbonate fuel cells and phosphoric acid fuel cells with slow start-up performance, PEMFCs operate at 60–80 °C with fast start-up, high power density, and excellent dynamic response [6]. So, this paper focuses exclusively on low-temperature PEMFCs for vehicle applications.

In PEMFCs, the anode exhibits simple hydrogen transport characteristics with lower flooding risk and low mass transfer resistance. In contrast, the cathode involves air supply, liquid water accumulation, and severe mass transfer limitations, which are the core factors affecting cell performance. Therefore, this study focused on cathode flow field optimization and did not discuss the anode flow field in detail.

As shown in Figure 1, PEMFCs are mainly composed of a polymer electrolyte membrane, catalyst layers (CLs), gas diffusion layers (GDLs), and bipolar plates (BPs) [7,8]. In a PEMFC, the polymer electrolyte membrane is primarily responsible for conducting protons, while preventing direct mixing of hydrogen at the anode and oxygen at the cathode, and blocking electron conduction to ensure that electrons can only form an electric current through the external circuit. The electrode of a PEMFC consists of the CL and GDL, featuring a typical porous diffusion electrode structure that combines reaction activity with mass transfer and electrical conductivity. The internal structure of the CL is rough, providing active sites for the electrochemical reactions of hydrogen and oxygen. The GDL possesses good porosity and electrical conductivity, which not only ensures uniform distribution of the reactant gases across the entire catalyst layer interface but also effectively conducts electrons and promptly removes the water generated by the reaction. As an integrated structural and functional component, the bipolar plate serves the roles of fluid distribution, current collection, and structural support.

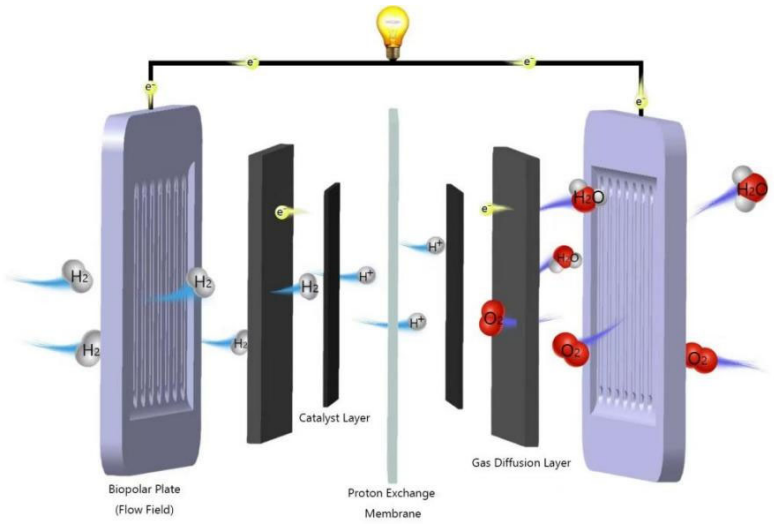


Figure 1. Schematic picture of the PEMFC.

The performance of PEMFCs is closely linked to their internal multi-physics fields, which include key aspects such as uniform distribution of reactant gases, proton conduction efficiency, water and thermal management, and product removal. Despite significant

progress in PEMFC research, many challenges remain. Fuel cells are needed to reduce pressure loss while ensuring uniform gas distribution, achieve a dynamic balance of water and thermal management under different operating conditions, and balance flow field performance with manufacturing costs to meet commercialization requirements [9]. Furthermore, as PEMFCs are applied on a large scale in areas such as automotive technology, their flow field design fulfills practical needs, including high power density, long service life, and resistance to harsh operating conditions.

Most existing reviews focused narrowly on conventional flow field optimization, single bionic designs or bipolar plate materials [10]. By contrast, this paper systematically reviewed the current research on PEMFC flow channel design and summarized the structural characteristics, performance advantages, and applicable scenarios of different flow field types, covering structures from traditional types to novel configurations.

2. Flow Channel Design

2.1. Geometric Structure Design of Flow Channels

2.1.1. Length, Width, Depth, and Aspect Ratio of Flow Channels

Flow channel geometric parameters (length, width, depth, aspect ratio, etc.) directly determined reactant transport, product water removal, pressure loss, current density uniformity, and temperature distribution [11], which were core optimization variables in PEMFC flow field design. The following provided a detailed analysis of the structural parameter optimization of three typical flow fields: parallel, serpentine, and interdigitated.

(1) Parallel Flow Field

For parallel flow fields, channel length was a key parameter affecting the liquid water transport process within the fuel cell. The generally accepted understanding was that, within the allowable pressure drop range, longer channels typically result in better water management. Xing et al. [12] developed a two-dimensional, non-isothermal, two-phase flow, anode partial flooding model, demonstrating that as channel length increased, the optimal cathode relative humidity rose, thereby enhancing cell performance. During 15 min of 0.5 A cm^{-2} steady-state operation, Bachman et al. [13] found that the longer 25 cm channels exhibited 18% higher maximum power density and 87% higher maximum current density than the shorter 5 cm channels. Moreover, the longer channel not only minimized water accumulation and achieved good performance but also required minimal extra power consumed by the auxiliary components of the fuel cell system.

Smaller rib and channel widths contributed to reduced ohmic resistance and superior cell performance. Goebel et al. [14] evaluated combinations of rib widths and channel widths of 0.25, 0.5, and 1.0 mm. Reducing the rib width down to the tested minimum of 0.25 mm improved cell performance compared with wider ribs. Scholta et al. [15] indicated that the optimal range for channel width or rib width was between 0.7 mm and 1 mm. When the dimensions became very small, the likelihood of channel blockage due to water droplet formation increased. In general, narrower channel dimensions were more suitable for high current densities, whereas wider channel dimensions performed better at low current densities. Lim et al. [16] divided the improved parallel flow channel into inlet, middle, and outlet sections. In their study, they increased the channel width in the outlet section. This generated a larger pressure drop in the collection region, thereby promoting the flow of reactants toward the outlet and improving water removal within the channel.

Shallow channel flow field plates performed better than deep channels because the pressure difference between adjacent channels in shallow channels was larger than that in deep channels. This led to increased under-rib convection and enhanced oxygen transport [17]. Using a two-dimensional anode model of a PEMFC, Xing et al. [18] also

found that increasing the channel depth reduced the liquid water saturation under the condition of short channel length. Wang et al. [19] developed a three-dimensional numerical model to investigate the influence of cathode parallel flow channel configuration on liquid water transport in a PEMFC. They found that at operating voltages below 0.7 V, a lower flow channel aspect ratio and a smaller channel cross-sectional area could enhance the liquid water removal rate, thereby improving cell performance.

(2) Serpentine flow field

For serpentine flow fields, changing the number of parallel channels to alter the path length of the PEMFC can affect its performance and uniformity. In general, a shorter path length provided a more uniform current density distribution. Shimpalee et al. [20] showed that as the path length increased, the pressure drop and water content also increased. The serpentine design with short flow channels achieved more uniform distributions of local temperature, water content and current density.

Apart from changing the path length, the optimization of the width, depth, and related derived parameters of the serpentine flow field was also of great significance for improving flow field performance and enhancing the electrochemical characteristics of the cell [21]. By adjusting channel width and height, it could reduce pressure loss, increase the oxygen content on the catalyst surface and achieve a uniform oxygen distribution within the catalyst [22]. For a triple-serpentine flow field design, Wang et al. [23] defined the channel width ratio η as the ratio of the total channel width to the total cell width. The researchers found that among the channel width ratios η of 0.4, 0.522 and 0.6, the device achieved the optimal performance at η = 0.6.

The channel-to-rib width ratio was an important parameter affecting the efficiency of PEMFCs. Under the condition of keeping the cell area and the number of channels unchanged, the channel width and the rib width exhibited an inverse relationship [24]. Kerkoub et al. [25] found that reducing the channel width and increasing the rib width could significantly improve the cell performance. When the channel-to-rib width ratio was reduced from 2.66 to 0.25, the performance of the serpentine flow field design was greatly enhanced by 20%. In addition, Wang et al. [26] used an isothermal two-phase three-dimensional model to investigate two serpentine flow fields with six and ten channels. They designed four-dimensional combinations consisting of channel width (W = 0.5 and 0.9 mm), channel depth (D = 0.5 and 1 mm), and rib width (B = 0.5 and 0.8 mm), as shown in Figure 2. The results indicated that narrower channel and rib widths were beneficial for enhancing under-rib convection, whereas a small channel cross-section led to an increased pressure drop in the flow field. Therefore, a synergistic balance between the two was required to achieve optimal flow field performance.

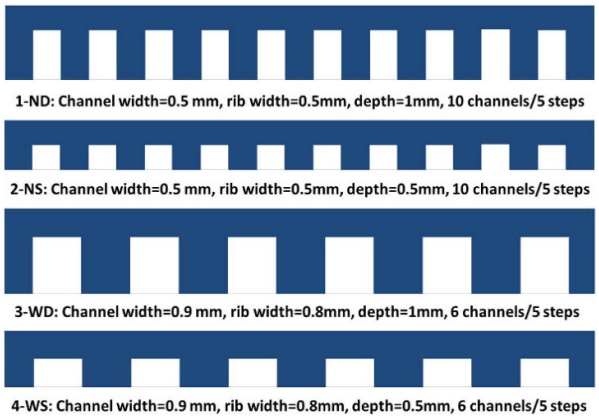


Figure 2. Geometric parameters of four different flow fields [26].

The optimization of flow channel depth and channel cross-section aspect ratio (defined as the height/width ratio) plays a significant role in the performance of PEMFCs. Manso et al. [27] found that at low operating voltages, cell performance was independent of the channel cross-section aspect ratio; at high voltages, as the channel cross-section aspect ratio increased, the mass transport rate was enhanced, thereby significantly improving cell performance. In addition, Zhang et al. [28] conducted research from the perspectives of peak power density and current density distribution. The results showed that under a channel width–depth combination of 1.2 mm–0.8 mm, the electrochemical performance of an eight-channel composite serpentine flow field PEMFC was superior to that of the 1 mm–1 mm width–depth combination. This confirmed the importance of properly matching the width and depth parameters to enhance cell performance.

(3) Interdigitated flow field

As one of the important types of PEMFC flow fields, the optimization of channel dimensions and the influence of related parameters on cell performance have also been extensively studied for the interdigitated flow field. Zhang et al. [29] investigated the effects of different outlet channel widths on cell performance and electrochemically active areas. The performance of the interdigitated flow field with 0.5 mm outlet channels was 18%, 10%, and 7% higher than 1 mm outlet at 0.75 V, 0.5 V, and 0.4 V, respectively. Chen et al. [30] established a two-dimensional model of an interdigitated flow field and simulated the effect of outlet channel width on the performance of a PEMFC. The results showed that the maximum molarity of oxygen at the outlet of 0.5 mm was 43.6% higher than that of 1 mm. They also resulted in more uniform electrolyte current density across the membrane cross-section and improved water removal capability.

Using a cathode channel with greater height led to a decrease in PEMFC performance. Since liquid water accumulates in the rib region, the larger the rib-to-channel width ratio is, the lower the cell performance. However, when the rib-to-channel width ratio was relatively large, the use of an interdigitated flow field design became more effective [31]. Wang et al. [19] found that for interdigitated flow field designs, the transport of reactants to the porous layer mainly relied on forced convection, and water was primarily removed by high shear forces. Consequently, the channel aspect ratio and cross-sectional area had a relatively small impact on cell performance. Cell performance first increased and then decreased with increasing aspect ratio or cross-sectional area. The channel aspect ratio for achieving optimal cell performance was 1.00.

2.1.2. Number of Flow Channels

The number of flow channels had a significant impact on cell performance, and this effect was particularly pronounced in serpentine flow fields. Depending on the number of channels, serpentine flow fields could be classified into single-channel serpentine flow fields and multi-channel serpentine flow fields [32]. Flow fields containing a smaller number of channels usually exhibited superior distribution uniformity and fuel cell performance.

Limjeerajarus et al. [33] compared single-channel serpentine, three-channel serpentine, and five-channel serpentine flow fields and found that flow fields with a smaller number of channels provided better uniformity and cell performance. When the number of channels was small, its impact on fuel cell performance was much greater than that of the flow field geometry. However, as the number of channels increased, the structure's influence became more significant. In a study of the number of channel branches in serpentine flow fields, Wang et al. [23] also compared the performance differences among single-serpentine, double-serpentine, and triple-serpentine flow fields. They clearly pointed out that the overall performance of the single-serpentine flow field was superior to that of the double-serpentine and triple-serpentine flow fields.

Liu et al. [34] designed two novel flow fields named the multistage serpentine flow field and the multistage parallel serpentine flow field. Compared with the three-channel serpentine flow field and the five-channel serpentine flow field, the average power densities of the two new flow fields increased by 0.687% and 1.256%, respectively.

Zou et al. [35] found that a fuel cell with a ten-channel serpentine flow field had a low operating pressure drop and suffered from poor under-rib mass transfer, which was unfavorable for outlet water drainage. Wu et al. [36] quantitatively analyzed the liquid water distribution in single-channel and four-channel serpentine flow fields. The results showed that when operated at a current density of 1000 $mA \cdot cm^2$, the single-channel configuration achieved 7% and 21% higher performance than its dual-channel and four-channel counterparts. Meanwhile, it exhibited a pressure drop around three times and seven times larger than the two structures above. In addition, the four-channel serpentine flow field was prone to severe flooding in the gas channels, leading to the largest voltage fluctuations.

2.2. Cross-Sectional Shape Design of Flow Channels

As the core carrier for reactant transport, product water removal, and current density distribution, the cross-sectional shape of the flow channel in a PEMFC directly affects key performance indicators such as cell performance, water management capability, and reactant utilization efficiency. Common flow channel cross-sectional shapes include rectangular, trapezoidal, parallelogram, triangular, stepped, semicircular, square, etc. Table 1 summarizes the advantages and disadvantages of various flow channel cross-sectional shapes.

Mohammedi et al. [37] showed in their study that the triangular channel cross-section exhibited the highest pressure drop, while the rectangular cross-section yielded the lowest. Compared with the channel geometry that has an inverted semi-elliptical bottom and an inverted trapezoidal top, the configuration with a trapezoidal bottom and an inverted trapezoidal top performed best and reduced the power density loss by 4.65%.

Triangular, trapezoidal, and semicircular channels significantly enhanced liquid water removal and improved oxygen utilization efficiency compared with rectangular channels [38]. Triangular and semicircular channel cross-sections can boost the output current of fuel cells by approximately 9%, thus enhancing their operating efficiency [39]. Among these, the triangular channel yielded the best cell performance, followed by the semicircular channel, trapezoidal channel, and rectangular channel in that order. Li et al. [40] also found that changing the cross-sectional shape of the serpentine flow channel from trapezoidal to triangular led to a higher local velocity of reactants near the gas diffusion layer. This resulted in increased oxygen concentration, more reaction heat, and higher current density, but reduced the uniformity of the current density distribution.

However, compared with parallelogram and trapezoidal shapes, the rectangular channel shape enabled the fuel cell to achieve a higher voltage and better performance. However, the trapezoidal channel cross-section was more favorable for reactant diffusion, allowing for a more uniform distribution of reactants. This led to a more uniform local current density within the reaction zone [41]. Sayan et al. [42] found that the inverted trapezoidal design achieved 3% higher power density than the square one at 0.45 V. Due to its smaller rib contact area and elevated ohmic resistance, the trapezoidal structure achieved the poorest performance across all test voltages.

In addition to the typical cross-sectional shapes, Liu et al. [43] were inspired by dome structures and designed a novel variable cross-section channel structure. This structure combined raised features with the traditional parallel channel design, which accelerated the flow of reactant gases and facilitated more effective entry of oxygen into the catalyst layer. This also resulted in more uniform distributions of oxygen and current density at the GDL and CL, thereby effectively improving the performance of the fuel cell.

Table 1. The advantages and disadvantages of various cross-sectional shape designs of flow channels.

Cross-Sectional Shape	View	Advantages and Disadvantages
Rectangular		Lowest pressure drop and high voltage, but poor water removal.
Trapezoidal		Favorable for reactant diffusion and uniform current density, but smaller rib contact area increases ohmic resistance.
Parallelogram		Moderate performance and less uniform reactant distribution than trapezoidal.
Triangular		Best cell performance and highest current output, but highest pressure drop.
Inverted trapezoidal		Improved water removal and higher power density than square, but higher pressure drop.
Semicircular		Better water removal and oxygen utilization than rectangular, but higher pressure drop.
Square		Standard baseline, but lower power density than inverted trapezoidal.
Dome		Stable voltage and stack temperature, but average water and oxygen transport.
Boot		Optimal pressure drop, heat and water management, but severe dehydration in galvanostatic operation.
Pentagon		A stably high pressure drop, but the lowest power density of all types.

Thapa et al. [44] investigated six channel cross-sectional shapes: square, trapezoid, dome, boot, pentagon and triangular. The results revealed that the boot-shaped cross-section achieved an optimal pressure drop of 23.9 Pa, along with superior oxygen distribution, water and thermal management, and net power output. At a high current of 35 A, the dome and square cross-sections maintained the highest and most stable potential, while also keeping the stack temperature well-balanced. The pentagon cross-section was prone to excessive cooling and water loss under high airflow conditions and achieved the lowest peak power density.

2.3. Baffle Design for Flow Channels

Inserting baffles into the cathode flow plate was a strategy to enhance oxygen diffusion and water removal inside the PEMFC. When fluid flowed through the baffle, the flow velocity underwent abrupt changes due to the disturbance, and the reactants were pushed into the catalytic layer. This enhanced internal mass transfer in the fuel cell and increased the reactant gas concentration in the flow channel. Compared with the conventional straight-channel flow field, baffles could significantly promote oxygen diffusion and water removal within the fuel cell, especially in the region around the baffles [45]. At high voltages, conventional channels adequately facilitated gas transport, and baffles showed minor mass transfer benefits. At low voltages, higher oxygen consumption led to oxygen deficiency in standard channels, while baffled flow fields improved oxygen transport and achieved superior performance [46]. A detailed analysis of baffle designs is presented below, based on factors such as baffle shape, size, and arrangement.

2.3.1. Baffle Shape

The most common baffle shapes were rectangles, trapezoids, triangles, squares, etc. Different baffle or blockage shapes exhibited different performance characteristics, and many researchers had studied various baffle shapes.

Wei et al. [47] found that at 0.5 V, the average current densities of PEMFCs were 984.3 mA/cm^2, 1184 mA/cm^2, 1165 mA/cm^2, and 1109 mA/cm^2, and the maximum power densities of PEMFCs were 0.601 W/cm^2, 0.755 W/cm^2, 0.703 W/cm^2, and 0.648 W/cm^2 for baffle-free, rectangular, trapezoidal, and semicircular baffles, respectively. Therefore, rectangular baffles achieved superior output performance.

Nevertheless, the output performance of some newly developed baffles was superior. Huang et al. [48] investigated the transport phenomena in flow channels with six different baffles. At an operating voltage of 0.4 V, cylindrical baffles yielded a current density of 1.82 A/m^2, which was 28%, 5% and 2.9% higher than the baffle-free, triangular and trapezoidal shapes, respectively. The current density distributions of the rectangular, triangular, stepped and trapezoidal shapes only presented marginal deviations.

Hong et al. [49] also studied and evaluated the effects of five representative baffle shapes on the flow characteristics and electrochemical performance of fuel cells. These shapes included a rectangular baffle, two variants of trapezoidal baffles, and two variants of triangular baffles. The results showed that rectangular and trapezoidal baffles exhibited the best performance at moderate blockage levels. In contrast, triangular baffles, due to their lower flow resistance, demonstrated better adaptability at high blockage levels.

2.3.2. Number, Height, and Angle of Baffles

In recent years, many researchers have conducted extensive studies on baffle structure design, parameter optimization, and performance influence mechanisms.

Increasing the baffle height improved mass transfer and increased output power. Perng et al. [50] found that using trapezoidal baffles with a large angle and large height could significantly improve local reactant transport, heat transfer efficiency, and liquid water removal efficiency in PEMFCs. Compared with a traditional gas channel without baffles, a novel gas channel equipped with trapezoidal baffles with an angle of 60° and a height of 1.125 mm could maximize the net power of the fuel cell by approximately 90%.

Researchers have made improvements based on conventional single baffles. Belchor et al. [51] proposed a parallel serpentine–baffle flow field plate design that could retain moisture in the flow channel, thus exhibiting better performance compared to the serpentine flow field plate. Wang et al. [52] also investigated a novel flow field structure with trapezoidal baffles arranged at unequal heights and unequal spacing. This structure could significantly

enhance the convection effect, thereby further improving the mass diffusion efficiency, water removal capability, and overall performance of the PEMFC. With the gradual increase in baffle height and reduction in baffle spacing, this design raised the maximum power density by 9.67% compared with the conventional baffle-free flow field.

Intelligent algorithms could be adopted to select the optimal baffle height for specific operating conditions and achieve the best optimization effect. Gao et al. [53] used an artificial neural network surrogate model combined with a non-dominated genetic algorithm II to optimize the blockage height in each channel. This method effectively reduced the liquid water volume fraction inside the flow channels and achieved superior water management capability, further increasing the net power density by 4.6%.

Increasing the number of baffles helped to enhance the mass flux and improve the uniformity of reactant distribution, but it also led to an increase in flow field pressure drop, which might consequently cause performance degradation of the PEMFC [54]. Ye et al. [55] showed that the output power density increased gradually as the number of baffles rose. For flow channel units with three, five, seven and nine baffles, the output power density grew by 8.22%, 11.10%, 13.77% and 14.91%, respectively. Meanwhile, the pressure drop also increased markedly, and the resulting pressure drop led to a significant increase in the extra power loss consumed by the auxiliary components of the fuel cell system. However, the increase in extra power loss was smaller than the increase in power output. Hong et al. [49] also showed in their study that while increasing the number of baffles promoted mixing and improved oxygen availability, excessive obstruction led to increased flow resistance, thereby reducing the performance gain.

The inclination angle of the baffle was also an important parameter affecting the output performance of the PEMFC. When the angle of the triangular baffle was set to 45°, the output performance of the fuel cell reached its peak. In addition, compared with the conventional serpentine flow field, when the output current density reached 0.8 A/cm^2, the power density of the 2° tapered channel was improved by a maximum of 12.65% [56,57]. Yin et al. [58] showed in their study that a larger leading angle of the baffle block led to a higher gas velocity component in the vertical direction, which could effectively enhance the convective transport of oxygen; however, it simultaneously reduced the convective area and oxygen delivery efficiency in the channel. A larger trailing angle of the baffle block induced the back-flow phenomenon at the rear of the baffle block, which led to the loss of gas pressure and poorer oxygen transport. The final results showed that when both the leading and trailing edge inclination angles were set to 45°, the trapezoidal baffle block achieved the best oxygen transport performance, and the corresponding fuel cell performance also reached its optimum.

2.3.3. Arrangement of Baffles

The arrangement of baffles or blockages had a significant impact on performance, with the staggered arrangement being the most widely used and effective. Figure 3 shows the staggered baffle arrangement.

To uniformly push the reactant species into the gas diffusion layer, Heidary et al. [59] placed blockage blocks in a staggered arrangement within the interdigitated flow field. The flow channel blockage increased the limiting current density and the maximum net power by 9% and 22%, respectively.

Wang et al. [60] found that both the parallel trapezoidal baffle flow field (PTBP) and staggered trapezoidal baffle flow field (STBP) generated over-baffle convection around the baffles, which was beneficial for mass transfer from the flow channel to the electrode. STBP flow fields also induced over-rib convection, further improving the uniformity of reactant distribution and water management capability. The maximum net power enhancement of

the STBP flow field reached 6.39% and 2.54% compared with the conventional parallel flow field and PTBP flow field, respectively.

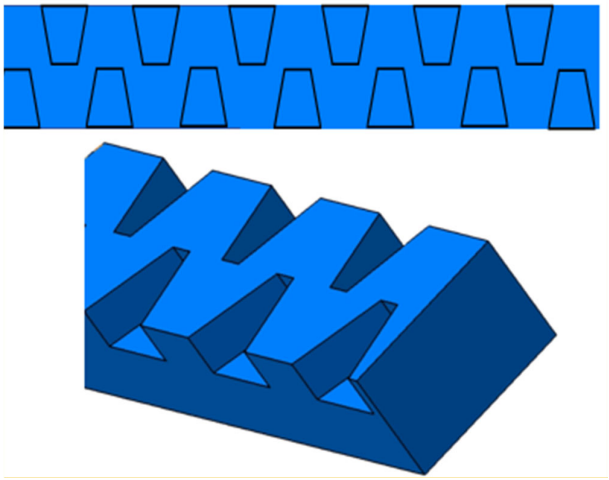


Figure 3. Schematic of the staggered arrangement of baffles [59].

2.3.4. Novel Baffle

In addition to traditional rectangular and trapezoidal baffles, some novel baffle structures have also been proposed to enhance fuel cell performance.

Liu et al. [61] proposed a novel helical baffle flow field and demonstrated that while inducing forced convection, the helical baffle generated cross-flow beneath the ribs, thereby enhancing oxygen supply in both directions. Subsequently, they found that a smaller pitch, larger diameter, and appropriate height and inclination angle could enhance the intensity of gas convection and effectively improve fuel cell performance. Compared with the conventional flow field, this novel flow field improved cell performance by 5.12% to 12.68% [62]. Cai et al. [63] studied a novel ship-like baffle cathode flow field, which could enhance mass transfer while generating relatively low extra power consumed by the auxiliary components. The sloping "bow" of the baffle helped to enhance mass transfer downward and the sloping "stern" of the baffle helped to further split the droplets already divided by baffles into smaller ones and threw them into the upper part of the channel. Yang et al. [64] proposed the water-drop curved baffle, which could effectively improve the overall performance of high-temperature PEMFCs, but also led to an increase in the pressure drop. The configuration with four baffles achieved superior performance, resulting in a net power density of 0.368 W/cm^2, which represented a 5.74% increase compared to the basic channel without baffles. Zhao et al. [65] also developed a low-resistance baffle structure inspired by a bionic airfoil. This structure significantly improved the uniformity of oxygen and gaseous water distribution while maintaining a low pressure drop and achieved a 6.28% performance increase over traditional designs.

Zhang et al. [66] designed a flow field with a half-baffle arrangement, which could reduce the pressure drop while maintaining current density distribution uniformity. Deng et al. [67] proposed an improved three-part trapezoidal baffle flow field and showed that the improved three-part baffle flow field could reduce the flow velocity near the baffles, thereby enhancing the mass transfer performance. The maximum net power of the novel flow field increased by 4.8% and 1.8% compared with the conventional parallel flow field and the ordinary trapezoidal baffle flow field, respectively.

In biomimetic flow field design, baffle structures also play an important role. Fahruddin et al. [68] investigated the effect of baffles on the performance of a PEMFC with a bio-inspired leaf flow field. While maintaining a moderate pressure drop, this design could guide fluid flow toward low-resistance regions, resulting in more uniform flow

distribution among the branches. The addition of baffles in the main channel increased the current density and power density of PEMFCs up to 18.29%. Based on a leaf vein biomimetic flow field structure with 10 branch channels on one side of the main channel, Xia et al. [69] added bionic streamlined blocking blocks inside the branch channels to construct a composite bionic flow field. The study found that the composite bionic flow field was beneficial for improving the performance of the PEMFC, and resulted in more uniform distributions of reactant gas and current density.

3. Flow Field Design

In a PEMFC, the substances generated by the electrochemical reaction mainly accumulate in the flow field on the cathode side of the bipolar plate. Meanwhile, the oxygen introduced to the cathode relies on the flow field structure to enhance its diffusion efficiency. The flow field design on the bipolar plate directly determines the transport pathways and distribution uniformity of the reactant gases (hydrogen, oxygen/air) over the electrode surface, while also affecting the removal efficiency of produced water and the stability of the temperature field inside the cell. These factors influence the mass transfer efficiency, water management capability, pressure drop, and power density of the fuel cell [70,71]. Therefore, the optimization of the cathode flow field in PEMFCs is crucial.

Conventional flow fields such as the parallel flow field (shown in Figure 4a), serpentine flow field (shown in Figure 4b), and interdigitated flow field (shown in Figure 4c) have received widespread attention in early research and practical applications due to their simple structures and ease of fabrication. However, each has obvious limitations: although the parallel flow field has low pressure loss, the uneven distribution of reactant gases could easily lead to flooding; the serpentine flow field enhanced water removal and gas mixing but suffered from high pressure loss and extra power loss consumed by the auxiliary components; and the interdigitated flow field improved mass transfer efficiency through forced convection but resulted in increased energy loss due to its structural characteristics [72,73]. To break through the performance limitations of conventional flow fields, novel flow field designs continued to emerge, including biomimetic flow fields based on the fluid transport characteristics of natural organisms, such as leaf-inspired bionic flow fields (Figure 4d), lung-inspired bionic flow fields (Figure 4e), and tree-inspired bionic flow fields (Figure 4f); 3D flow fields that utilized three-dimensional spatial structures to optimize mass transfer; metal flow fields that employed metallic materials to enhance electrical conductivity and mechanical strength; and composite flow fields that combined the advantages of multiple conventional flow fields, among others [74]. These novel flow fields had shown significant potential in improving gas distribution uniformity, which provided a new technical pathway for PEMFC performance improvement. Table 2 summarizes the advantages and disadvantages of various flow fields.

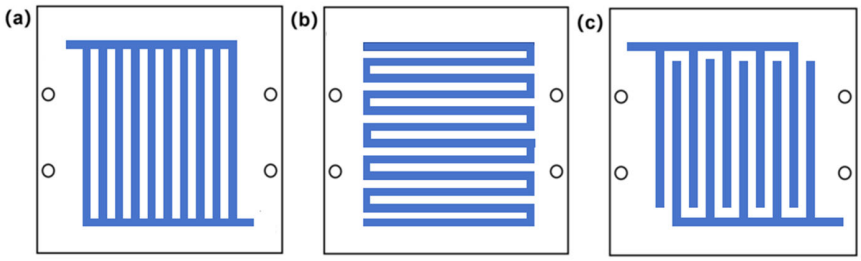


Figure 4. *Cont.*

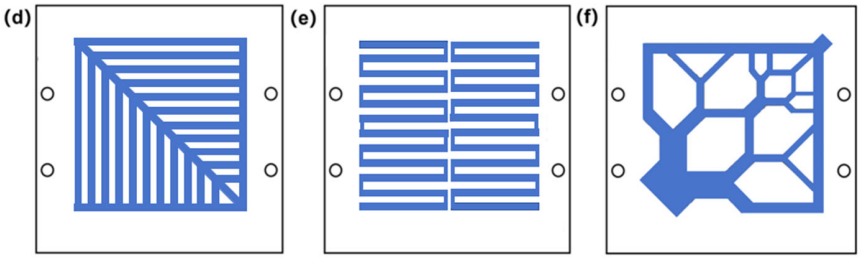


Figure 4. Schematic diagrams of typical flow field structures for PEMFCs: (**a**) parallel, (**b**) serpentine, (**c**) interdigitated, (**d**) leaf-inspired bionic, (**e**) lung-inspired bionic, and (**f**) tree-inspired bionic.

Table 2. The advantages and disadvantages of various flow field designs.

Flow Field Design		Advantages	Disadvantages	Author and Year
Parallel Flow Field		Low pressure drop, easy fabrication and low production cost	Severe rib flooding and uneven gas distribution under high current	Pellegri et al., 1980 [75]; Wang et al., 2012 [76]; Chen et al., 2022 [77]; Wang et al., 2022 [78]; Wang et al., 2022 [79]; Tian et al., 2024 [80]; Fu et al., 2025 [81]; Velisala et al., 2018 [82]; Qi et al., 2002 [83]
Serpentine Flow Field		Uniform reactant supply, reliable water removal and mass transfer	High overall pressure drop and excessive auxiliary pumping loss	Babay et al., 2024 [84]; Enearu et al., 2018 [85]; Dong et al., 2019 [86]; Kaiser et al., 2025 [87]; Zuo et al., 2025 [88]; Boni et al., 2025 [89]; Suresh et al., 2011 [90]; Abdulla et al., 2021 [91]; Duc et al., 2025 [92]; Saminathan et al., 2023 [93]; Zhang et al., 2026 [94]
Interdigitated Flow Field		Forced convection and optimal anti-flooding at high density	High flow resistance and possible GDL mechanical damage	Wang, 2015 [95]; He et al., 2000 [96]; Yan et al., 2006 [97]; Hu et al., 2004 [98]; Wang et al., 2004 [99]; Hu et al., 2009 [100]; Bhattarai et al., 2019 [101]; Mohammadtabar et al., 2016 [102]; Peng et al., 2011 [103]; Peng et al., 2011 [104]; Moslemi et al., 2022 [105]; Deng et al., 2024 [106]; Asadi et al., 2024 [107]
Composite Flow Field		Combine the advantages of multiple structures	Complex channel design and difficult fabrication	Hamrang et al., 2022 [108]; Fan et al., 2025 [109]; Gao et al., 2024 [110]; Sevinc, 2026 [111]
Metal Flow Field		High mechanical strength, excellent electrical/thermal conductivity and high volumetric power density	Corrosion issues and potential long-term durability concerns	Makkus et al., 2000 [112]; Tawfik et al., 2007 [113]; Wu et al., 2025 [114]; Awin et al., 2019 [115]; Makkus et al., 2000 [116]; Wang et al., 2004 [117]; Tanaka et al., 2014 [118]; Gao et al., 2023 [119]; Li et al., 2024 [120]; Kim et al., 2026 [121]; Wang et al., 2026 [122]; Wu et al., 2024 [123]
Novel Flow Field	Conical	Overcome flooding at low flow rate, and strengthen oxygen transport	May cause uneven velocity distribution	Ghasabehi et al., 2021 [124]; Timurkutluk et al., 2018 [125]; Huang et al., 2022 [126]; Chowdhury et al., 2017 [127]; Chowdhury et al., 2018 [128]
	Wavy	Generate flow disturbance and enhance oxygen transport	Excessive pressure loss and insufficient oxygen supply	Kuo, 2006 [129]; Li et al., 2026 [130]; Ding et al., 2020 [131]; Seyhan et al., 2017 [132]; Chen et al., 2025 [133]; Wang et al., 2025 [134]; Wang et al., 2026 [135]
	Intersectant	Uniform distribution of reaction mediums	Complex self-similarity regions and difficult fabrication	Wen et al., 2017 [136]; Ma et al., 2025 [137]
	Zig-zag	Homogenize reactant gas distribution and boost internal mass transfer efficiency	Raise pressure drop due increased number of bends	Li et al., 2025 [138]
	Pin	Low pressure drop and uniform reactant distribution	Prone to flow stagnation zones and water accumulation	Zaffora et al., 2024 [139]; Dang et al., 2025 [140]; Tan et al., 2025 [141]
	Spiral	Generate secondary vortices and strengthen heat and mass transfer	Complex curved passages and high pressure drop	Jang et al., 2012 [142]; Yao et al., 2023 [143]

Table 2. *Cont.*

Flow Field Design		Advantages	Disadvantages	Author and Year
Bio-Inspired Flow Field	Leaf-shaped	Uniform gas distribution, low pressure drop and efficient water drainage	Branch channels prone to water blockage	Zheng et al., 2025 [144]; Wang et al., 2026 [145]; Kloess et al., 2009 [146]; Kang et al., 2019 [147]; Dong et al., 2020 [148]; Xiao et al., 2025 [149]; Huang et al., 2024 [150]; Zhu et al., 2025 [151]; Ghadhban et al., 2021 [152]; Wang et al., 2025 [153]; Fahruddin et al., 2019 [154]; Lian et al., 2020 [155]
	Lung-shaped			
	Lung-shaped	Low pressure drop, better reactant transport and water removal	Complex fractal branching and weak anti-flooding capacity	Muñoz-Perales et al., 2023 [156]; Bethapudi et al., 2021 [157]; Ghanbari et al., 2024 [158]; Xie et al., 2026 [159]; Lu et al., 2024 [160]
	Spider-web			
	Tree-shaped	Low flow pressure drop, uniform fluid distribution and large effective active area	Weak anti-flooding capacity and susceptible to liquid water blockage.	Stephenson et al., 2015 [161]; Wan et al., 2023 [162]; Tan et al., 2022 [163]; Liu et al., 2025 [164]; Lorenzini-Gutierrez et al., 2013 [165]; Damian-Ascencio et al., 2017 [166]; Chen et al., 2023 [167]
Self-humidifying Flow Field		Enhance proton conductivity and improve low-humidity performance	Pore flooding under high current densities and local gas starvation	Jiang et al., 2026 [168]; Lian et al., 2022 [169]; Lian et al., 2023 [170]; Qiao et al., 2024 [171]; Wang et al., 2024 [172]; Tong et al., 2021 [173]

In recent years, researchers both domestically and internationally have conducted extensive and in-depth studies on PEMFC flow field design. Most researchers compared the characteristics and overall performance of different flow fields by examining factors such as flow distribution, velocity distribution, concentration distribution, and pressure drop within the flow channels. For example, Maia et al. [174] studied commonly used flow field designs, serpentine, double-serpentine, parallel, interdigitated, and pin-type, and examined the concentration distribution, velocity distribution in the porous regions of the fuel cell, and the pressure drop in the flow channels, using computational fluid dynamics modeling. Wang et al. [175] compared the performance of six flow field configurations using a modified general model: (a) single serpentine, (b) two-path serpentine, (c) three-channel serpentine, (d) six-channel serpentine, (e) parallel, and (f) interdigitated. Their results quantitatively and systematically demonstrated that different flow field designs significantly affected flow distribution and pressure drop. Therefore, it was clear that flow field design had a significant impact on various aspects of PEMFC performance, and the industry had already implemented several improvement measures to enhance its performance. A systematic analysis of each conventional flow field design and its improved novel flow field designs is presented below.

3.1. Parallel Flow Field

The parallel flow field design was first patented by Pollegri and Spaziante in 1980 [75]. It consisted of multiple parallel path channels directly connected to the channel inlet and outlet, and it was one of the most basic flow channel configurations on the bipolar plate of a fuel cell. The parallel flow field evenly distributed the fluid into multiple parallel channels, which could reduce the pressure drop and featured a simple structure with low processing cost. However, the parallel flow channel suffered from uneven flow resistance, and under high current conditions, problems such as uneven reactant distribution and weak water removal capability occurred [76]. Typically, the following measures were adopted to improve the conventional parallel flow field in order to address the above issues.

3.1.1. Auxiliary Channels

Compared with the porous electrode beneath the flow channel, the porous electrode beneath the rib region faced lower local oxygen concentration and more severe flooding

issues. Researchers have integrated auxiliary under-rib channels into the parallel flow field to address this problem.

Based on innovative improvements to the conventional parallel flow field, Chen et al. [77] and Wang et al. [78] designed a novel flow field structure by embedding auxiliary channels inside partially hollow ribs and drilling a series of arrayed holes in the auxiliary channels, as shown in Figure 5. This novel flow field design effectively enhanced battery performance under high current density while maintaining good electrical conductivity. Through reasonable optimization of the flow field geometry and the number and length of the auxiliary channels, further improvements in battery performance and current uniformity could be achieved with very low pressure loss, laying the foundation for subsequent enhancement of battery performance and optimization of the flow field.

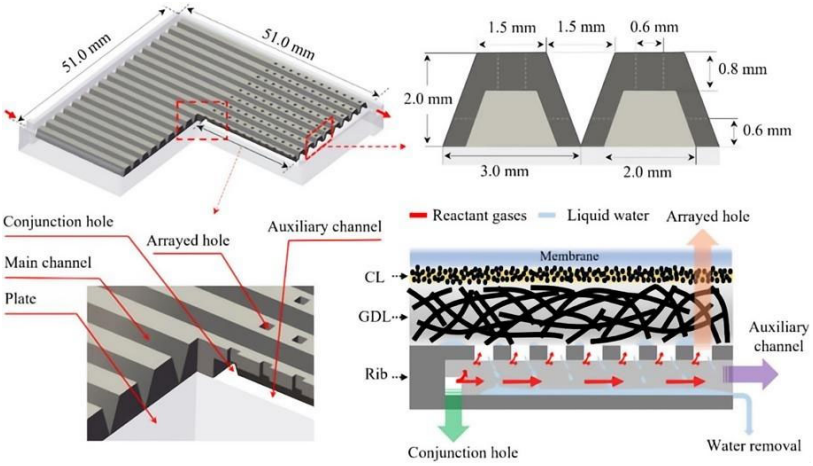


Figure 5. The parallel flow field design with auxiliary channels [78].

The coupling optimization scheme that combined auxiliary channel design with other optimization strategies generally achieved a greater performance improvement than single optimization methods. This "synergistic effect" could break through the optimization bottleneck of a single variable and realized a significant leap in the macroscopic performance of the cell.

Wang et al. [79] analyzed and compared conventional parallel flow fields, wave flow fields, and auxiliary wave flow fields. The results indicated that the periodic wave structure and auxiliary channels generated dual-region forced convection, forcing more reactants to be transported to the gas diffusion layers beneath both the channels and the ribs, thereby significantly improving cell performance.

Tian et al. [80] developed a coupling-optimized parallel flow field PEMFC that combines under-rib auxiliary channels with a gradient-porosity GDL. The auxiliary channels enhance gas mixing and uniform distribution, improving oxygen mass transfer; the porosity gradient enhances capillary water drainage and alleviates flooding. Compared with a conventional parallel flow field, the synergistic effect led to a 16.7% increase in maximum power density and a 20.6% expansion in current range. Its performance was significantly superior to that achieved by single-structure optimization.

3.1.2. Double-Path Flow Field

The dual-path flow field was primarily equipped with two sets of independent gas inlet and outlet ports, with the inlet of one flow passage located near the outlet of the other. Moreover, in any segment of the electrode active area, the reactants in adjacent channels flowed in opposite directions, allowing the dry inlet gas to directly acquire moisture from the adjacent wet channel. This not only made better use of the water generated by the fuel

cell itself to humidify the dry reactants, but also eliminated the uneven reactant distribution problem of conventional single-path designs [81,82].

Figure 6 illustrates a double-path-type flow field design. Qi et al. [83] proposed a dual-path flow field design and demonstrated that this design allowed the incoming dry gas to become humidified by acquiring some moisture from the exhausted wet gas. Moreover, in any part of the active area, the drier gas in one flow path could share moisture from the wetter gas flowing in the other flow path. By comparing the single-path design with the dual-inlet and dual-outlet design, Lim et al. [15] showed that the multi-inlet and multi-outlet design achieved more uniform fluid distribution and a gradual pressure drop from the inlet to the outlet, which helped improve the performance of the PEMFC.

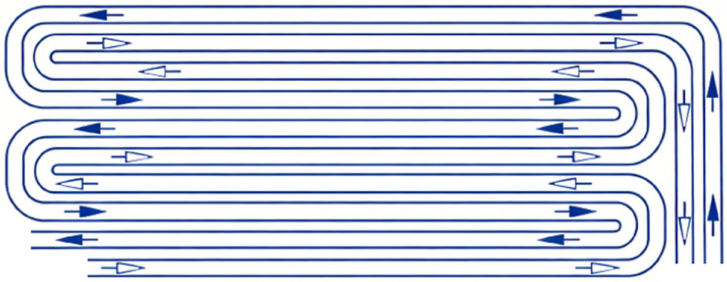


Figure 6. A double-path-type flow field design: solid and empty arrows were used to show the flow of reactant [83].

3.2. Serpentine Flow Field

The classic serpentine flow structure featured an unbroken main channel. On the flow field plate, the channel formed successive 180° bends, directing reactant gas to sweep over the electrode surface in a winding route. Such a curved layout covered the entire electrode active region, delivering uniform reactant supply, reliable water removal, and excellent mass transfer performance. However, as the reactant gas flows along the serpentine channel, it is continuously consumed by the catalyst layer, causing the gas concentration to gradually decay along the flow direction [84]. In addition, the long single channel with multiple turns generated substantial frictional and bend-related flow losses. A prominent pressure gradient existed from the inlet to the outlet, and the overall pressure loss was much higher than that of parallel flow designs [85]. Accordingly, relevant improvements were implemented on the conventional serpentine flow field to resolve the aforementioned problems.

3.2.1. Number of Channel Bends

The flow field structure directly determines the mass transfer efficiency of the reactant gases and the liquid water removal capability. With its continuously bent channel structure, the serpentine flow field can generate high flow velocities and strong shear forces within the channels, enabling efficient liquid water transport [86].

As a critical structural parameter of serpentine flow fields, the quantity of channel bends exerts a remarkable influence on the temperature uniformity, output properties, and water management performance of fuel cells. Moderately increasing the number of bends helped to extend the gas coverage within the flow field and improve the uniformity of current density distribution. However, an excessive number of bends could increase flow resistance, leading to a higher pressure drop, which ultimately reduces the overall performance of the fuel cell [87].

Wang et al. [23] found that increasing the number of bends reduced the equivalent cross-sectional area of the channel, thereby increasing the reactant flow velocity under the same inlet flow rate. In addition, more channel corners enhanced flow disturbance, forcing

more oxygen to penetrate into the GDL. This improved the local oxygen mass flow rate and utilization efficiency, consequently enhancing the cell output performance.

Zuo et al. [88] found that the five-bend channel structure yielded 7.2%, 27.9% and 35.3% higher net power density than the parallel flow field, conventional serpentine flow field, and two-bend channel structure, respectively. The findings indicated that appropriately raising the bend count effectively elevated cathode oxygen levels and optimized the uniformity of oxygen distribution, thereby achieving better comprehensive mass transfer performance compared with conventional flow field structures.

3.2.2. Novel Serpentine Flow Field

To enhance the performance of serpentine flow fields, researchers have proposed many other novel optimization strategies.

Boni et al. [89] investigated several novel channel designs, including a wide serpentine flow field, a single-serpentine flow field, a wavy serpentine flow field, and a split serpentine flow field. Among the various channel configurations, the split serpentine flow field showed the best performance, while the wavy serpentine flow field exhibited the poorest performance. The branched structure of the split serpentine flow field enabled a more uniform distribution of reactant gases and reduced the pressure drop across the flow field, thereby helping to improve performance and energy efficiency and extend the service life of the fuel cell. Based on the conventional split serpentine flow field, Suresh et al. [90] proposed a novel flow field layout called the Enhanced Cross-flow Split Serpentine Flow Field (ECSSFF). This structure enhanced cross-flow in regions prone to flooding, efficiently removing liquid water accumulated at the bends. It achieved uniform reactant distribution across the active area of the cell and a low pressure drop throughout the flow field, effectively reducing the extra power loss consumed by the auxiliary components. In a recent study, Abdulla et al. [91] extended the ECSSFF channel layout to a square cross-sectional cell. The study found that the square cross-sectional PEMFC with a four-channel ECSSFF design on the cathode side outperformed the five-channel serpentine flow field. Benefiting from a stronger cross-flow effect, this structure achieved a more uniform reactant distribution over the catalyst layer, resulting in a 10% increase in current density at 0.3 V, a 6.5% improvement in peak power density, and a 20% reduction in channel pressure drop.

Based on the conventional serpentine flow field, Duc et al. [92] developed novel U-shaped and L-shaped flow field designs. Among these, the U-shaped structure featured low pressure drop and good under-rib convection and the L-shaped structure had more bends and exhibited a higher pressure drop but offered advantages in enhancing forced convection. The enhanced under-rib convection increased oxygen concentration in the GDL and reduced the water content, thereby improving both the water content within the membrane and the uniformity of current density. Janaki et al. [93] achieved an improvement by dividing the conventional serpentine flow field channel into three segments. In each segment, the channel length first decreased and then increased, allowing for a smoother gas flow path. The improved novel flow field achieved more uniform gas distribution and better water management, resulting in higher power output.

In a recent study, Zhang et al. [94] proposed a novel Conjugate Bionic Double-Serpentine Flow Field structure. The curved channels and rounded corner structures reduced the risk of liquid water stagnation, enabling smoother gas–liquid transport within the channels and effectively mitigating flooding issues. Compared with the conventional serpentine flow field, the conjugate double-serpentine flow channel structure effectively shortened the gas transport path and enhanced the turbulence effect within the channels. It increased the oxygen transport velocity by 30.9% and effectively improved the gas supply and distribution uniformity in the reaction zone.

3.3. Interdigitated Flow Field

The interdigitated flow field was composed of two groups of parallel, staggered channels, namely inlet and outlet passages. The two sets of channels were arranged alternately, with the channel ends closed. These channels were placed in an alternating pattern with sealed ends. Gas was unable to travel straight along the channels and had to cross the gas diffusion layer under the ribs, moving sideways from inlet passages to outlets before exiting. In the GDL, the transport mechanism of some reactant gases changed from diffusion to forced convection, forcing the reactants to flow completely through the diffusion layer [95,96].

The forced transverse convection caused the gas to pass through the entire GDL and CL. Such cross-flow improved reactant distribution across the CL, and the elevated flow speed helped to eliminate accumulated liquid water in relevant areas. This alleviated the cathode electrode flooding issue, and thus significantly enhanced the current density. Therefore, the performance of the interdigitated flow field was generally superior to that of the conventional parallel flow field [97,98].

However, the interdigitated flow field had discontinuous channels and multiple dead ends. Although it enhanced convective mass transfer within the porous electrode, the forced convection of reactant gases through the diffusion layer generated a large pressure drop. At the same time, due to the relatively high gas flow velocity, the gas diffusion layer might be damaged, leading to a decline in fuel cell performance [99]. Typically, the following measures are adopted to improve the conventional interdigitated flow field to address the above issues.

3.3.1. Slotted Design

In 2009, Hu et al. [100] first proposed a slotted-interdigitated flow field. Researchers cut grooves on the ribs of standard interdigitated flow fields in this new design. The structure maintained the core characteristics of traditional interdigitated configurations and eliminated the fully closed layout of original ribs. It improved mass transfer efficiency in the CL and reduced flow resistance, resulting in a pressure drop significantly lower than that of the conventional interdigitated flow field. In addition, this design provided drainage channels for liquid water, suppressing flooding and reducing pressure loss [101,102].

In this design, the clamping force between the GDL and the flow field plate caused non-uniform compression of the GDL. This led to GDL intrusion into the reactant gas channels, which significantly affected flow distribution. This problem prompted numerous scholars to carry out further research on such slotted structures. Figure 7 illustrates the slotted-interdigitated flow field. Peng et al. [103] divided the middle section of this slotted-interdigitated flow field into three regions and proposed an optimization scheme: the slot depth in the central channels should be smaller than that in the side channels, while the slot width should be larger than that in the side channels. This could effectively eliminate the uneven flow distribution and achieve higher reaction performance [104].

3.3.2. Novel Interdigitated Flow Field

To enhance the performance of interdigitated flow fields, researchers have also proposed many novel optimization strategies.

In their study on liquid water transport within the compressed microporous layer and GDL of a PEMFC with an interdigitated flow field, Moslemi et al. [105] found that the drainage duration reached the best state at a porous transport layer compression rate of 85%. In addition, a thicker microporous layer lowered the liquid water volume inside the porous transport layer. These conclusions provide references for subsequent flow field optimization work.

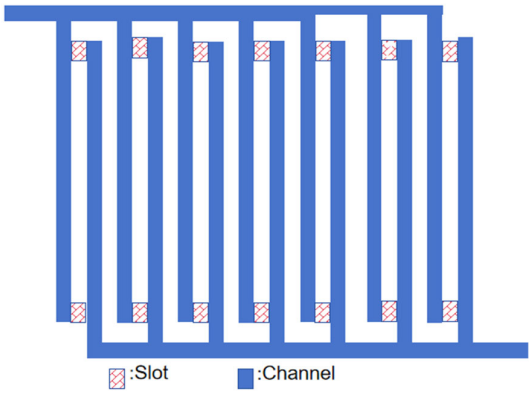


Figure 7. The slotted-interdigitated flow field [103].

Deng et al. [106] proposed a porous-channel interdigitated flow field structure. The results showed that, compared with the interdigitated flow field, the porous-channel interdigitated flow field could further increase the dissolved water content in the cathode catalyst layer. This improved the water retention performance and mass transfer efficiency of the PEMFC under low humidity conditions. At the same time, it reduced ohmic losses and concentration losses, resulting in a 7.8% improvement in cell performance. Asadi et al. [107] compared the wavy interdigitated flow field with serpentine, conventional interdigitated, tapered interdigitated, and spiral interdigitated flow fields. The results showed that the wavy interdigitated flow field possessed the strongest reactant convection and diffusion transport capabilities, significantly improving the reaction rate and power density. It also achieved uniform water saturation and reduced the likelihood of flooding.

3.4. Composite Flow Field

Composite flow fields integrate the features of two or more distinct flow channel structures on a single bipolar plate. It can reduce pressure drop and improve reactant mass transfer efficiency and water management capability, thereby optimizing cell performance and stability. Combining flow fields with different geometric structures and functional characteristics was an effective and universal design approach to overcome the inherent limitations of a single flow field configuration. In recent years, researchers have explored novel composite flow field schemes to fully combine the strengths of different channel designs.

The novel serpentine–interdigitated composite flow field adopted a unique structural layout. At the inlet section, only the middle flow channel remained open, whereas the bilateral channels were sealed. Conversely, the central channel was closed at the outlet, while the lateral channels were kept unobstructed. This innovative structure leveraged the pressure gradient among adjacent channels to induce intensive forced cross-rib convection. The proposed flow configuration substantially strengthened the internal mass transfer behavior and achieved homogeneous oxygen distribution across the catalyst layer. Meanwhile, it mitigated liquid water saturation and alleviated the water flooding phenomenon [108].

Fan et al. [109] developed a novel composite flow field by integrating the respective characteristics of the conventional serpentine flow field and the interdigitated flow field. Only partial uneven distribution of liquid water saturation emerged at the outlet region, which prevented the occurrence of localized water flooding. Due to the very complex channel design, the pressure drop was between that of the serpentine flow field and the interdigitated flow field. Moreover, the complex flow channel structure increased the difficulty and cost of manufacturing, which had become a key direction for subsequent optimization and improvement of this novel composite flow field.

In a recent study, Gao et al. [110] found that in the combined block and sub-channel flow field, the flow velocity in the main channel increased significantly when the fluid encountered the blocks, forcing more oxygen to penetrate through the GDL and reach the CL. Furthermore, the sub-channels assisted in fluid transport, increasing the oxygen concentration beneath the ribs and consequently improving the uniformity of oxygen distribution.

Sevinc [111] proposed a novel composite flow field structure named "ser-pin", which integrates the geometric features of serpentine and pin-type channels. The innovative composite structure efficiently weakens internal concentration gradients, improves the contact efficiency between reactants and catalyst surfaces, and facilitates homogeneous temperature distribution across the reactive zone. Although the increased channel complexity led to a slight rise in pressure drop, the overall performance improvement was significant, compensating for the shortcomings of traditional single flow fields.

3.5. Metal Flow Field

The bipolar plate is one of the key components of a PEMFC. They undertake multiple critical functions, including the uniform delivery of fuel and air and the isolation of internal gas and coolant leakage. In early research, graphite was widely adopted for bipolar plate fabrication, owing to its excellent electrical conductivity and corrosion resistance. Nevertheless, graphite-based bipolar plates possessed unavoidable limitations, such as high fabrication expenses, inferior mechanical performance, and low volumetric power density. In contrast, metallic thin plates exhibited outstanding mechanical stability, superior electrical and thermal conductivity, as well as excellent stamping formability, compared with traditional graphite counterparts [112]. Currently, aluminum, stainless steel, titanium, and nickel are often considered as possible alternative materials for bipolar plates in PEMFCs [113].

Wu et al. [114] added nickel foam into the channels of a parallel flow field, using the nickel foam as a flow distribution layer to completely replace the channels and ribs on the cathode. The nickel foam flow field could eliminate local mass transfer bottlenecks, achieve uniform distribution and efficient transport of oxygen and product water, and significantly reduce the risk of flooding under high current density. Awin et al. [115] used aluminum foam as the flow field. Compared with the graphite bipolar plate, the conversion efficiency was 9.9% higher for the metal foam design, and its weight was 27.8% lower.

Nowadays, stainless-steel materials have garnered extensive research interest, owing to their high mechanical strength, excellent chemical stability, low gas permeability, great scalability for mass production, and cost advantages. More critically, stainless-steel bipolar plates presented low corrosion rates and enabled PEMFCs to maintain stable output performance over thousands of operating hours. Therefore, stainless steel is a highly promising bipolar plate material [116,117]. Tanaka et al. [118] used a stainless-steel corrugated mesh as both the flow field and the GDL. Experimental results demonstrated that this unique structure mitigated the water flooding problem effectively.

To enhance the performance of metal flow fields, researchers have also proposed many novel optimization strategies. Combining the metal foam flow field with other flow fields yielded a new flow field with better performance and effectively addressed the drawbacks of the original flow field. Gao et al. [119] combined the metal foam flow field with the traditional rib flow field and proposed a composite foam–rib flow field structure. This flow field improved oxygen transport and water drainage capability beneath the ribs, thereby increasing oxygen concentration and current density.

Li et al. [120] proposed a composite foam/serpentine flow field that combined the enhanced transport characteristics of the metal foam flow field with the well-defined main flow direction of the serpentine flow field. Its maximum power density was significantly

higher than those of the metal foam flow field and the parallel serpentine flow field. Kim et al. [121] also found that this novel flow field combined the directional convection of the serpentine channel with the multi-directional diffusion in the metal foam, improving reactant transport and mitigating concentration losses under high-load operation.

In a recent study, Wang et al. [122] proposed a novel metal foam–leaf vein stratified flow field, successfully addressing the issues of uneven reactant distribution in metal foam flow fields and the persistent under-rib transport limitations or constraints imposed by specific inlet/outlet arrangements in bio-inspired flow fields. Building upon the original metal foam flow field, Wu et al. [123] integrated a fractal manifold into the metal foam flow field design. Compared with the conventional metal foam flow field, this novel design achieved better cell performance, lowered mass transfer resistance, and consistently maintained lower liquid water content.

3.6. Novel Flow Field

3.6.1. Conical Flow Field

Conical flow fields are generally divided into two types: converging and diverging. The flow channel converges or diverges linearly along the flow direction. Such structural characteristics overcome the water flooding defect that easily occurs in traditional parallel flow fields under low-flow-rate operating conditions. Meanwhile, the conical layout strengthens oxygen delivery from flow channels to the CL and substantially mitigates the mass transfer restriction of fuel cell reactions. This provides a new approach for the structural optimization of parallel flow fields in PEMFCs [124].

Timurkutluk et al. [125] improved the conventional parallel flow field structure using converging and diverging design concepts. The improved tapered parallel flow field achieved superior mass transfer and water drainage capacities compared to conventional parallel flow configurations. This optimized structural design successfully boosted the peak power density of fuel cells by 16%, achieving a remarkable performance advancement for PEMFCs. Huang et al. [126] proposed a novel conical serpentine flow field that promoted droplet aggregation and rapid removal and maintained excellent water management. By optimizing the corner structure of flow channels, the modified design significantly enhanced mass transfer efficiency and gas distribution uniformity in contrast to conventional serpentine flow fields. The optimized configuration increased the maximum power density by 3.75% and reduced the cathode pressure drop by 58.4%.

Chowdhury et al. [127] designed the inclined channel depth from the inlet to the outlet of the serpentine flow field in four different specifications (1.5 mm–0.5 mm, 2.5 mm–1.5 mm, 3 mm–1.0 mm, 3.5 mm–0.5 mm). Experimental results show that the converging flow field (1.5 mm–0.5 mm) enhanced the power density of fuel cells by 16% and exhibited the best performance. In a follow-up study, Chowdhury et al. [128] found that reducing the channel depth facilitates better reactant diffusion and reduces water concentration in the reaction zone. It also strengthened oxygen transport, which elevated fuel concentration within the confined channel space. Furthermore, the reduction in the depth gradient between inlet and outlet passages further improved current density values and realized a more consistent current distribution across the cell surface.

3.6.2. Wavy Flow Field

The cross-sectional dimensions of wavy flow channels shrank periodically during gas operation, which produced a vertical flow component for reactant gases, changed the internal fluid motion path, and enhanced flow disturbance. This structural optimization strengthened oxygen transportation toward the cathode GDL and CL and water management capability, and efficiently improved the internal mass transfer efficiency within flow

channels [129]. Many researchers both domestically and internationally have conducted extensive studies on wavy flow channels, developing a variety of optimization strategies that provide new pathways for improving performance.

Li et al. [130] found that the wavy flow field significantly increased local gas flow velocity. The periodic flow disturbances induced by the waveform structures effectively facilitated both lateral and longitudinal mass transport. Ding et al. [131] further found that in a parallel flow field, the adoption of wavy gas channels enhanced the peak power density of fuel cells by 13.44%. However, oxygen delivery in interdigitated and serpentine flow fields relied primarily on secondary convection. This inherent transport characteristic greatly weakened the positive optimization effects of wavy channel structures, so the performance of cells showed no obvious enhancement.

The potential of wavy flow fields has not yet been fully explored. Seyhan et al. [132] investigated the effect of sinusoidal wavy channels with different amplitudes on the performance of PEMFCs. Wavy channels with a small amplitude could utilize the wave structure to induce flow oscillation, enhance oxygen diffusion capability, and promote water drainage. They simultaneously reduce associated losses and exhibit better performance than wavy channels with a large amplitude.

In a recent study, Chen et al. [133] designed a novel composite flow field structure by combining the serpentine flow field with the wavy flow field. This flow field promoted the uniform distribution of reactant gases and current density and facilitated rapid water flow. Wang et al. [134] comparatively studied the parallel flow field, sinusoidal wave flow field, opposite sinusoidal wave flow field, and staggered opposite sinusoidal flow field. Compared with the conventional parallel flat flow field, the novel staggered opposite sinusoidal flow field consistently outperformed the other three structural designs and achieved a 9.46% improvement in net power output. In addition, Wang et al. [135] further optimized the structural design of wavy flow channels, proposing variable cross-section wavy flow channels. Compared with conventional wavy flow channels, the variable cross-section wavy channel structure effectively improved water removal efficiency and addressed the issues of excessive pressure loss and insufficient oxygen supply in conventional rectangular wavy channels.

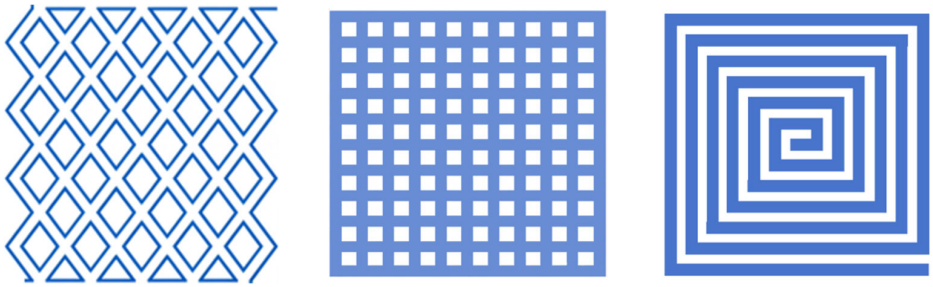
3.6.3. Other Novel Flow Fields

Figure 8a shows the intersectant flow field. Wen et al. [136] proposed a novel intersectant flow field for metal bipolar plates in PEMFCs. In this design, there were independent exits and inlets for each single self-similarity intersectant region to ensure the uniform distribution of reaction media or products, enabling higher power and current densities compared to the single-serpentine flow field. Ma et al. [137] proposed a rhombic flow field with an intersecting structure, in which the originally straight channel edges were modified into three types of inward-curved structures. The optimized structure maximized the peak power density of proton exchange membrane fuel cells, with a maximum performance improvement of 6.78%.

Li et al. [138] optimized the conventional straight parallel flow channels of a PEMFC by incorporating a zigzag geometry. The zigzag structural design homogenized the distribution of reactant gases within flow channels and significantly boosted the internal mass transfer efficiency of reactants. The design, equipped with a 45-degree, seven-bend zigzag, achieved a 10.1% enhancement in peak power output.

Figure 8b shows the pin flow field, which exhibits characteristics such as low pressure drop and uniform reactant distribution. It could generate local vortices, enhance convective mass transfer to the CL, and improve reaction efficiency and power density [139]. However, it was prone to forming flow stagnation zones, and water easily accumulated in low-

velocity regions. Dang et al. [140] analyzed the characteristics of liquid water accumulation, transport, and removal in the cathode of a fuel cell with a hexagonal pin flow field. The hexagonal pin flow field generated a more uniform and stronger velocity in the Y-direction. This led to excellent performance even under very low pressure loss, which facilitated the uniform distribution of reactants and water [141].



(**a**) (**b**) (**c**)

Figure 8. Schematic diagrams of novel flow field structures: (**a**) the intersectant flow field [136], (**b**) pin flow field, (**c**) spiral flow field.

Figure 8c shows the spiral flow channel. Jang et al. [142] conducted a numerical simulation of the performance of a PEMFC with a spiral flow channel and experimentally validated the numerical predictions. Compared with the serpentine flow fields, the spiral channel structure generated secondary vortexes. This strengthened the heat and mass transfer effects inside curved flow passages and increased the average current density by 11.9%. In order to improve the related design, Yao et al. [143] in the present work proposed a new spiral flow field with a bypass. The reaction gas entered the flow field in the central path and diffused in two directions through the flow channel and the bypass. This structural optimization expedited oxygen transportation across flow passages and elevated the overall oxygen utilization efficiency of the fuel cell system.

In a recent study, Liang et al. [176] designed a five-inlet radial flow field bipolar plate to address the poor stackability of radial flow fields. The results showed that under the same operating conditions, this structure achieved lower pressure loss and higher current density and power density than conventional serpentine and parallel flow fields. Increasing the branch channel width and decreasing the rib width can improve gas distribution uniformity and reduce the risk of blockage.

3.7. Bio-Inspired Flow Field

The flow field inside the bipolar plate plays a crucial role in controlling flooding, ensuring proper water management within the cell, preventing flooding, and improving cell performance under high current density. Bio-inspired flow field designs based on Murray's Law—which states that the cube of the main channel diameter equals the sum of the cubes of the secondary channel diameters to minimize energy consumption—have attracted extensive attention from researchers due to their ability to effectively distribute fluids, as well as their low pressure drop and good water management [177,178]. The formula of Murray's law is shown in Equation (4).

$$r_0{}^3 = r_1{}^3 + r_2{}^3 + r_3{}^3 + \cdots \quad (4)$$

3.7.1. Fractal Flow Field Design

In 2004, Tüber et al. [179] first proposed the multi-channel fractal design based on the combination of fractal distribution channels and parallel transport channels. This new fractal approach achieves uniform and continuous flow distribution while reducing

pressure drop by using a multi-branch structure with biological fluid channels. However, the channels of the fractal system were prone to water blockage, leading to uneven reactant distribution. The performance of PEMFCs with fractal channels was superior to a parallel design but inferior to a serpentine design.

Cho et al. [180] also proposed a finite element model of a PEMFC with a fractal-branching, lung-inspired flow field, and determined the effect of the branch generation number N on GDL thickness and fuel cell performance. The fractal flow field contained self-similar, repeatedly branching H-shaped channels, allowing a single inlet to branch into 4^N outlets via flow paths of equal length. This enabled the use of a thinner GDL and improved the uniformity of reactant concentration at the flow field interface. Trogadas et al. [181] demonstrated in their study that lung-inspired fractal flow fields with branch generation numbers N = 3 and N = 4 reduced the pressure drop by 75% and 50% relative to conventional serpentine designs, reducing the power consumption required for reactant pressurization and recirculation. At current densities above 0.8 $A \cdot cm^{-2}$, the flow field with N = 4 generations homogenized reactant distribution in the CL, improving cell performance by 20% and 30% under 50% and 75% RH, respectively.

Despite the fact that fractal flow field layouts enhanced fuel cell performance via uniform gas distribution and reduced internal entropy generation, they possessed several non-negligible limitations: 1. fractal flow structures exhibited weak anti-flooding capacity and were susceptible to liquid water blockage, which triggered inhomogeneous gas dispersion and unstable current output [182]; 2. the shape and size of the flow channels imposed stringent requirements on manufacturing, limiting their fabricability.

Therefore, further refinement and optimization by researchers are still needed in the future. Bethapudi et al. [183] employed a function of polarization technique to detect the internal hydrodynamics of two different fractal flow field PEMFCs, namely one-way and two-way fractal PEMFCs. These were achieved by monitoring the corresponding acoustic activity generated by them. The results showed that the two-way fractal PEMFC had a larger contact area between the flow field and the MEA, and lower ohmic resistance than the unidirectional fractal structure. However, it exhibited relatively higher acoustic activity and was affected by cell flooding. In contrast, although the one-way fractal flow field had a smaller contact area, it allowed water to be directly discharged from the cell surface.

3.7.2. Bio-Inspired Design

In recent years, bio-inspired design has become an important direction for the optimization of bipolar plate flow channels. Through millions of years of natural selection and evolution, the natural fluid distribution systems in plants and animals have developed highly optimized structures, enabling critical functions such as fluid transport, substance distribution, and waste removal with extremely high efficiency. These functions are highly consistent with the core missions that bipolar plate flow channels are required to undertake [184]. In nature, the leaf vein networks of plant leaves, the airway branching of human lungs, and tree-like branching structures, by virtue of their unique branching configurations and fractal characteristics, achieve uniform fluid distribution and low-resistance transport. They also achieve efficient mass exchange within confined spaces, facilitating uniform reactant distribution and better water management [185,186].

Many researchers have begun to investigate the influence of nature-inspired flow fields on the performance of PEMFCs. Common types of bio-inspired flow fields include leaf-shaped, lung-shaped, tree-shaped, and novel biomimetic flow fields. Each type of flow field is analyzed individually below.

Leaf-Shaped Flow Field

The leaf vein system of plant leaves exhibits a typical fractal branching structure. The main vein serves as the core channel, branching stepwise into secondary and tertiary veins, ultimately extending to every region of the leaf. This hierarchical branching design enables uniform transport of water and other nutrients, as well as efficient oxygen removal, characterized by low resistance, uniform distribution, and good transport performance [144]. Based on the leaf vein system of plant leaves, the leaf-shaped flow field ensured that the reactant gases more uniformly covered the entire electrode active area and that the velocity, pressure, and reactant concentration on the catalyst surface were more evenly distributed. It also formed efficient water drainage pathways, significantly reducing flooding problems and reactant supply deficiencies [145].

In 2009, Kloess et al. [146] first proposed a leaf-like flow field (for specific structural details, refer to Kloess et al. [146]). The leaf-type flow field exhibited lower pressure loss than the single serpentine and interdigitated flow patterns, and its gas distribution to the GDL was more uniform.

The performances of bio-inspired flow fields based on different plant leaves vary significantly.

Kang et al. [147] developed and simulated reticulate vein flow fields based on ginkgo biloba leaves and dicotyledonous plant leaves (for specific structural details, refer to Kang et al. [147]). The ginkgo leaf flow field exhibited a 40% higher net power density than conventional parallel flow channels and a 21% higher net power density than dicotyledon leaf flow fields. Meanwhile, its inlet power consumption was merely 3% of that required by traditional serpentine flow channels.

Based on bio-inspiration principles and Murray's law, Dong et al. [148] designed a bio-inspired flow field structure using the four-leaf clover plant as the natural biological prototype (for specific structural details, refer to Dong et al. [148]). This novel flow field plate not only improves the uniformity of reactant gas distribution and reduces the pressure drop within the channels, but also increases the maximum output power by 114% compared to a parallel flow field fuel cell.

Xiao et al. [149] designed a bio-inspired flow field structure using the vein structure of gardenia leaves (a dicotyledonous plant) as the bionic prototype (for specific structural details, refer to Xiao et al. [149]). Increasing the inlet channel width reduced the gas flow velocity and prolonged the reactant residence time. As the angle increased, the power tended to rise slowly.

Huang et al. [150] adopted a leaf-vein-like structure and proposed the leaf bionic flow field (for specific structural details, refer to Huang et al. [150]). The main channel outlet of this flow field was tapered and had a segmented three-stage structure. The design took drainage requirements into account, and the newly added straight channels could effectively remove liquid water from the channels and enhance mass transfer.

Zhu et al. [151] also designed a leaf-shaped biomimetic flow field. Compared with parallel and serpentine flow fields, the leaf-shaped flow field improved power density by 12.89% and 4.31%, respectively. For this flow field, the average liquid water saturation in the GDL and the pressure drop was lower than that of the serpentine flow field. At the same time, both the reactant transport efficiency and the uniformity of oxygen distribution on the catalyst layer surface were significantly improved. Ghadhban et al. [152] also proposed a novel leaf vein flow field derived from biological systems. The biomimetic flow field lacked straight-through channels between the inlet and outlet, which increased the pressure difference and forced water to flow through the GDL. Therefore, the average reactant flow velocity and concentration within the GDL, as well as the water management capability, were significantly improved.

The leaf-shaped design has shown promising potential for supplying air reactants in PEMFCs. The inlet width of the main channel and the angle between the main and secondary channels significantly affected the performance of the biomimetic flow field. Increasing the main channel inlet width and optimizing the bifurcation angle could notably improve reactant distribution uniformity. Consequently, many researchers have investigated structural improvements of the leaf-shaped flow field.

Wang et al. [153] found that the angle between the main and secondary channels could regulate the fluid flow velocity and the temperature distribution. An angle of approximately 25° yielded the best performance, but resulted in a higher pressure drop. Increasing the channel height and width could enhance water management capability while reducing the pressure drop and improving reactant distribution uniformity. However, this led to an increase in the membrane electrode assembly voltage and temperature, as well as a decrease in the outlet reactant concentration. Fahruddin et al. [154] indicated that channel width in a biomimetic flow field affected reactant transport efficiency. Reasonably increasing the channel width at the inlet of the main channel made the oxygen concentration distribution on the cathode side more uniform, thereby ensuring more stable oxygen supply. This optimized design could increase current density and power density by 5.49% and 5.55%, respectively. Lian et al. [155] established a three-dimensional isothermal single-phase model of a leaf-vein-inspired biomimetic flow channel and conducted experiments using a single cell. The study found that appropriately increasing the angle between the main channel and the sub-channels helped improve oxygen distribution uniformity and facilitated the removal of excess water, thereby enhancing PEMFC performance.

The number of branches is also a major factor affecting the leaf-shaped flow field. Xia et al. [67] designed an improved leaf vein biomimetic flow field by taking advantage of the characteristics of the leaf vein network structure. The results showed that the leaf vein biomimetic flow field offered significant advantages, including lower pressure drop, more uniform reactant gas distribution, and higher output power. Among the designs, the leaf vein biomimetic flow field with 10 branch channels on one side of the main channel achieved the best output power, which was 5.894% higher than that of the conventional serpentine flow field.

Lung-Shaped Flow Field

The trachea served as the primary channel and successively branched into bronchi, enabling air to reach every part efficiently. It facilitated rapid gas exchange of oxygen and carbon dioxide, while blood carried away the exchanged gases in a timely manner. The lung-inspired flow field was a biomimetic channel design that drew on the transport morphology of biological lungs, combining the geometric advantages of serpentine and interdigitated flow fields. It achieved higher current density at lower pressure losses [156].

In 2009, Kloess et al. [146] first proposed the lung-inspired flow field (for specific structural details, refer to Kloess et al. [146]) and analyzed a 25 cm^2 cell unit based on the lung design through numerical simulation and experimental testing. The lung-inspired flow field exhibited lower pressure drop, improved reactant transport, and enhanced water removal capability. Under operating conditions of 65–75 °C, 2 atm back pressure, and 100% relative humidity, its peak power density was up to 30% higher than that of the conventional serpentine flow field. Bethapudi et al. [157] showed in their study that the lung-inspired flow field fuel cell exhibited higher surface temperature, better electrochemical performance, and more uniform current distribution. In contrast, the single-serpentine flow field fuel cell suffered from non-uniform current distribution due to cell flooding. Furthermore, the single-serpentine cell experienced flooding, while the lung-inspired cell did not.

Based on the lung flow field, researchers have proposed many new flow field designs. Ghanbari et al. [158] proposed a converging–diverging lung-shaped serpentine (CDLIS) flow field consisting of two symmetrical lung-like structures and a repeating contraction–expansion pattern (for specific structural details, refer to Ghanbari et al. [158]). The CDLIS possessed efficient mass transfer capability, stronger convective effects, and excellent current density, enabling the most effective water management. Furthermore, it effectively reduced the risk of flooding and significantly improved output power.

Xie et al. [159] proposed a novel expanding–straight–contracting flow field (for specific structural details, refer to Xie et al. [159]). Compared with the conventional serpentine flow field and CDLIS, it enhances membrane hydration and liquid water expulsion, increasing oxygen mole concentration, oxygen distribution uniformity, and net power, thereby significantly improving the output performance of the PEMFC. In a recent study, Lu et al. [160] designed a lung-inspired hybrid flow field with three functional layers. These layers were the reactant distribution layer, directional transport layer, and water removal layer, which together formed a multistage H-type bifurcation structure. The results show that, compared with the conventional parallel flow field, the maximum net power density increased by 16.55%. Moreover, this structure achieved more effective mass transfer, better velocity distribution, more efficient water management, and more favorable pressure drop characteristics.

Tree-Shaped Flow Field

The tree-shaped flow field originated from the natural tree-like branching systems found in nature, such as tree roots and branches. This flow field featured a hierarchical structure of a main channel, secondary channels, and terminal branches. It had consistent morphology and branching angles across different levels, composed of units of the same shape [161]. Currently, there are three common types of tree-like fractal network structures, T-shaped, Y-shaped, and H-shaped, as shown in Figure 9. These basic microchannels can be fabricated and combined into complex fractal tree-like channel networks [162].

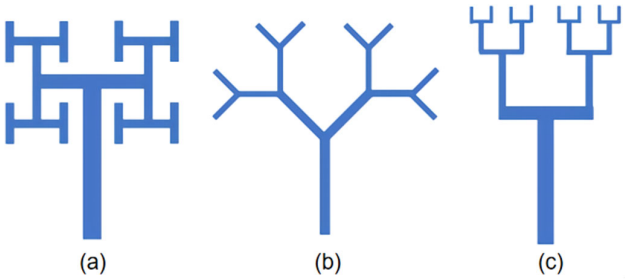


Figure 9. Schematic diagram of three fractal tree-like structures: (**a**) H type, (**b**) Y type, and (**c**) T type [162].

Tan et al. [163] proposed a novel Y-shaped tree-like flow field based on the design concepts of Constructal Theory and Murray's law. This new flow field effectively reduced parasitic losses caused by pressure drop within the flow channels, thereby achieving energy savings for the fuel cell system. Wan et al. [162] further investigated the flow field of a PEMFC with a Y-shaped tree-like fractal structure. Derived from Murray's law, the optimal angle of 75° for symmetric bifurcating flows was proven suitable for fuel cell flow field design, improving the transport characteristics of reactant gases and the overall performance of PEMFCs. Liu et al. [164] adopted an H-shaped tree-like fractal structure at the flow field inlet to construct a novel flow field. This inlet fractal configuration initiated primary branching at the base fractal node, was subdivided into two secondary branched channels, and was further extended to form tertiary fractal structures. In comparison with

composite serpentine flow fields, this innovative design facilitated more homogeneous distribution of hydrogen and oxygen reactants within the cell.

Tree-like flow structures achieve the advantages of low flow pressure drop and uniform fluid distribution. Increasing the bifurcation levels of tree-shaped layouts expanded the effective active reaction area, which helped fuel cells attain higher current density and power output [165]. Damian-Ascencio et al. [166] also considered four different dendritic structures. The number of leaf vein bifurcations and their inclination angles were used as characterization parameters. The results showed that the structure with a secondary bifurcation angle of 37° was highly efficient in removing water from the cathode flow channel, thereby generating favorable current density. Furthermore, by increasing the number of bifurcations, the PEMFC produced higher current density and lower entropy generation. Chen [167] also proposed a novel tree-shaped fractal cooling flow field for fuel cell bipolar plates. This flow field not only achieved better coolant distribution and temperature uniformity but also successfully addressed the issue of excessive pressure drop in the cooling flow field, thereby reducing power loss.

Other Types of Biomimetic Flow Field Designs

To improve water management performance and the uniformity of reactant distribution in fuel cells, researchers have developed various biomimetic structures.

Xie et al. [187], inspired by the spider-web structure, proposed a novel spider-web-type flow field. In this flow field, the polygon shape and the number of spiral channel layers were key design parameters. Although at high current densities its voltage and power density were lower than those of the serpentine flow field, it exhibited a lower pressure drop and better oxygen distribution and water removal. This avoided the limitation of the serpentine flow field caused by excessive pressure drop. Guo et al. [188] also proposed an optimized design of a spider-web biomimetic flow field. Compared with the serpentine flow field, when the spiral channels and diagonal channels were symmetrically arranged on the main channel connecting the inlet and outlet, the peak current density increased by 2.31%. Meanwhile, the pressure loss was reduced by 96.07%, which helped improve oxygen utilization efficiency and thereby reduced the operating cost of the fuel cell.

This flow field exhibited good fluid distribution and heat transfer uniformity. Wang et al. [189] found that the spider-web-inspired channel significantly reduced high-temperature regions on the membrane while optimizing the water content distribution, minimizing its variation. Fan et al. [190] integrated the structures of interdigitated flow fields and conventional spider-web flow fields to propose a biomimetic spider-web flow field. The results indicated that increasing the number of inlets and outlets, making the main inlet flow channel intermittent, and interconnecting the main outlet flow channels significantly improved water distribution and reduced pressure drop within the porous electrodes.

Liu et al. [191] proposed a bamboo-inspired flow channel and integrated it into the cathode side of an air-cooled PEMFC. The introduction of bamboo nodes induced localized flow disturbances that enhanced the intensity of multi-physics field transport. Compared with the conventional parallel flow channel, the bamboo-inspired configuration improved the output by 2.17%. Parameter optimization showed that increasing the length, width, and number of bamboo nodes further improved power output and transport uniformity.

Wang et al. [192] proposed and designed a bio-inspired auxiliary fishbone-shaped flow field. This novel flow field significantly enhanced under-rib mass transfer and water removal capability, and made reactant and saturation distributions more uniform, thereby improving fuel cell efficiency and operational stability.

Cai et al. [193], inspired by the fins of cuttlefish, designed a bio-inspired wave-like structure and applied it to the flow channels of a fuel cell. The results showed that compared

with conventional straight channels, this wave-like channel altered the flow direction and velocity of the gas and made it easier for reactants in the central region of the channel to diffuse into the GDL, thereby increasing the current density. Moreover, compared with ordinary wave-like channels, this novel channel structure preserves flow space on both sides of the channel, thus reducing flow resistance and effectively decreasing the pressure drop.

These research results demonstrate that bio-inspired structures can indeed play a positive role in the design of flow fields for PEMFCs, thereby enhancing electrochemical performance. This provides new ideas for the development and innovation of flow fields.

To improve mass transport efficiency while reducing pressure loss in PEMFCs, Wang et al. [194] proposed a bionic fish-scale porous flow field. At an operating voltage of 0.2 V, this structure reduced the pressure drop by 44.92% compared with the serpentine flow channel and raised the current density by 36.58% relative to the parallel flow channel. At 0.4 V, its peak power density was improved by 8.13% and 27.82% versus the serpentine and parallel flow channels, respectively. Zhou et al. [195] proposed a bio-inspired lotus-root-shaped flow field design, which combined wavy main channels with sub-channels. Compared with the conventional parallel flow field, this structure significantly promoted under-rib transport through transverse inter-rib paths and improved the spatial uniformity of multi-physics field distributions.

Inspired by the arc-shaped structure and staggered arrangement of fish scales, Chen et al. [196] designed a fish-scale-based biomimetic flow field. It featured wider sub-channel inlets, and its arc-shaped geometry helped fluid flow more smoothly from the main channel into the sub-channels. Compared with conventional parallel flow fields, this flow field design achieved a 9.3% rise in power density and a 5.47% decrease in pressure drop.

3.8. Self-Humidifying Flow Field

Appropriate humidification was found to enhance proton conductivity and reduce ohmic resistance for PEMFCs, thereby increasing output power and overall efficiency. Furthermore, a steady-state humidified environment inside the fuel cell allowed the generated water to uniformly wet the entire CL, promptly replenishing dry spots caused by local high temperatures or high current densities. This maintained the integrity of proton transport pathways within the CL, thereby accelerating electrochemical reactions. Therefore, precise control of the water content in the fuel cell system was considered crucial for improving system stability and reliability [168].

Among existing flow field designs for fuel cells, porous flow fields have been found to exhibit excellent self-humidifying performance due to their highly controllable pore space and structural flexibility. Lian et al. [169] proposed a novel porous flow field architecture based on metallic fibers featuring continuous capillary channels and strong capillary suction. This structure effectively retained moisture and enhanced the back diffusion of water vapor from the cathode to the anode, thereby achieving self-humidification. At 50 °C, when the porosity was optimized to 70%, the flow field increased the limiting peak power density by 18.75%.

Lian et al. [170] found that by adopting a diffusion channel configuration with a width of 1 mm, a spacing of 7 mm, eight channels, and type-A geometry (type A was perpendicular to the direction of the flow field inlet and outlet lines), the optimized fiber-based porous self-humidifying flow field fuel cell achieved a peak power density of 0.810 W/cm^2, which represented a 15.21% increase over the original design.

Qiao et al. [171] adopted a patterned alkaline CL in the cathode. By optimizing the water management mechanism, they significantly improved the fuel cell performance under low-humidity conditions. When the patterned alkaline CL was distributed at a ratio

of 25% in the central region of the cathode, the resulting fuel cell achieved a peak power density of 1.02 $W \cdot cm^{-2}$ at 10% relative humidity, which was 31.72% higher than that of a cell without the alkaline CL. Wang et al. [172] introduced a novel CL structure composed of a one-dimensional TiO_2 nanoarray and Pt/C catalyst. Under low-humidity conditions, it achieved a peak power density of 689.36 $mW \cdot cm^{-2}$, which corresponded to 93% of the performance obtained at 100% RH.

Tong et al. [173] designed a self-humidifying channel, as illustrated in Figure 10. This design blended low-humidity and high-humidity gases inside self-humidification channels to balance gas humidity, thereby optimizing water and heat distribution within the PEMFC. When the self-humidifying flow channel was positioned at a distance of 5 mm from the centerline, the cross-convection flow channel achieved optimal water–heat distribution and output performance.

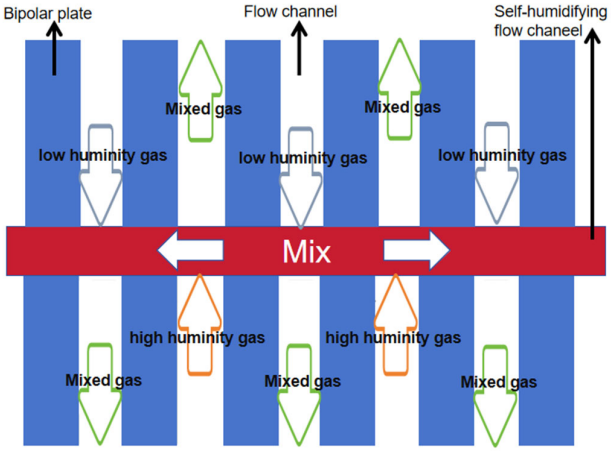


Figure 10. Schematic diagram of self-humidifying flow channel: the solid line represents the self-humidifying flow channel [173].

3.9. Commercial Application Status

Among overseas manufacturers, the first-generation Toyota Mirai adopted a fish-scale-like three-dimensional fine-mesh flow channel on a coated stainless-steel substrate, achieving high volumetric power density. The second-generation model switched to planar cathode channels with a tapered structure to reduce manufacturing costs. The Honda Clarity used corrugated wavy flow channels combined with a counter-flow arrangement to enhance under-rib convection and self-humidification [197]. The Hyundai NEXO applied a composite flow field structure that combines slotted serpentine and interdigitated finger-like patterns [198]. Ballard installed graphite multi-serpentine flow fields in its stationary stacks and upgraded its heavy-duty products to metallic serpentine channels with a tapered cross-section.

Domestic enterprises have mainly applied three types of flow fields in commercial vehicles: multi-serpentine, width-tapered, and wavy designs. Weichai Power adopted segmented tapered serpentine channels in its heavy-duty truck stacks. SinoHytec developed a solution combining standard serpentine channels with auxiliary under-rib channels for medium-power stacks. SAIC and SHPT (Shanghai Hydrogen Propulsion Technology) have installed partially width-tapered wavy flow fields on their passenger car prototypes.

For industrial selection, 3D or metallic wavy flows were preferred for compact passenger cells and cost-saving tapered/wavy structures prevailed for domestic heavy-duty vehicles [199].

4. Three-Dimensional Flow Field

The three-dimensional (3D) flow field passed through the undulating spatial structure, which endowed the gas flow field with velocity components both in the plane and vertical directions of the membrane electrode, thereby enhancing the convective mass transfer of gas toward the CL. In recent years, 3D flow fields for fuel cells have attracted the attention of researchers. This paper introduced 3D flow fields in detail, classifying them into 3D fine-mesh flow fields, 3D graphene foam flow fields, 3D metal foam flow fields, and other new types of 3D flow fields.

4.1. Three-Dimensional Fine-Mesh Flow Field

Mirai from Toyota developed a 3D fine-mesh flow field, which improved water management and mass transport in the fuel cell stack. As a result, it had drawn extensive scholarly attention and research [200].

Kim et al. [201] first proposed a two-phase model of PEMFCs considering Forchheimer's inertial effect to investigate the liquid water and mass transfer behavior inside the 3D complex flow field PEMFC. They found that the 3D complex flow field enhanced the liquid water removal capability within the flow channels and promoted liquid water removal from the GDL. Furthermore, the special structures could disturb fluid flow and induce convection phenomena. This significantly increased the oxygen concentration in the CL region, thereby enhancing output power under high-current-density conditions.

Figure 11 illustrates the three-dimensional fine-mesh flow field. Zhang et al. [202] also found that a three-dimensional refined mesh flow field could achieve a more uniform distribution of reaction rates within the CL by significantly increasing the mass transfer area between the GDL and the flow field, alongside a design featuring perpendicular flow of hydrogen and air.

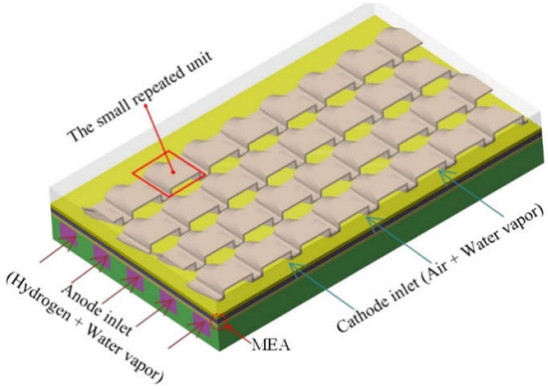


Figure 11. Schematic of PEMFC with 3D fine-mesh flow field [202].

Yu et al. [203] constructed a three-dimensional multiphase computational fluid dynamics model of a PEMFC incorporating a 3D fine-mesh flow field. The 3D fine-mesh flow field consisted of divided cells and collection grooves. These flow channels featured a contracting section and a gradual height variation, causing the gas to undergo repeated splitting, merging, and disturbance. Therefore, this structure reduces the angle between the gas flow and mass transfer direction, enhances oxygen concentration and distribution uniformity, and improves water removal capability.

In a recent study, Sun et al. [204] established a PEMFC model with a 3D fine-mesh flow field and investigated it using a three-dimensional computational fluid dynamics model. The results showed that as the porosity of the 3D fine-mesh structure increased, the local flow velocity rose and the oxygen partial pressure drop decreased. Based on the traditional flow field, Sun et al. [205] proposed three novel three-dimensional flow fields: a

metal foam flow field, a fine-mesh flow field, and a wire-mesh flow field. Compared with two-dimensional flow fields, the three-dimensional flow fields not only significantly enhanced the mass transfer process and improved output performance but also induced forced convection of the fluid, further enhancing the diffusion and dispersion of reactant gases.

4.2. Three-Dimensional Graphene Foam Flow Field

Graphene foam is composed of an interconnected, flexible graphene network that can serve as a transport pathway for charge carriers. This material simultaneously possesses the structural advantages of metal foam and the unique characteristics of graphene. Therefore, since the flow field was made solely of graphene, the corrosion issues associated with metal foam were no longer a concern [206].

Park et al. [207] applied graphene foam as the flow field in PEMFCs to enhance cell performance under high-current-density conditions. This compressed graphene foam formed smaller in-plane pores and more tortuous reactant transport paths within the membrane electrode assembly, thereby accelerating the diffusion rate of reactants into the gas diffusion layer. Furthermore, the graphene foam MEA exhibited lower mass transport resistance than conventional MEA because the graphene foam was more favorable for the transport of reactants and water.

Conventional serpentine flow field designs employed two-dimensional channels and rib structures, which often led to water accumulation, hindering reactant transport and interfering with water removal. However, in the study by Jang et al. [208], hydrophilic polymer grafting into the patterned region of 3D multilayered graphene (MLG)-coated Ni foam was proposed to improve water management in fuel cells, as shown in Figure 12. The cell provided gas transport paths through the hydrophobic surface of graphene and direct water removal paths through the patterned hydrophilic regions. This design consequently improved mass transfer and boosted PEMFC performance under high-current-density conditions.

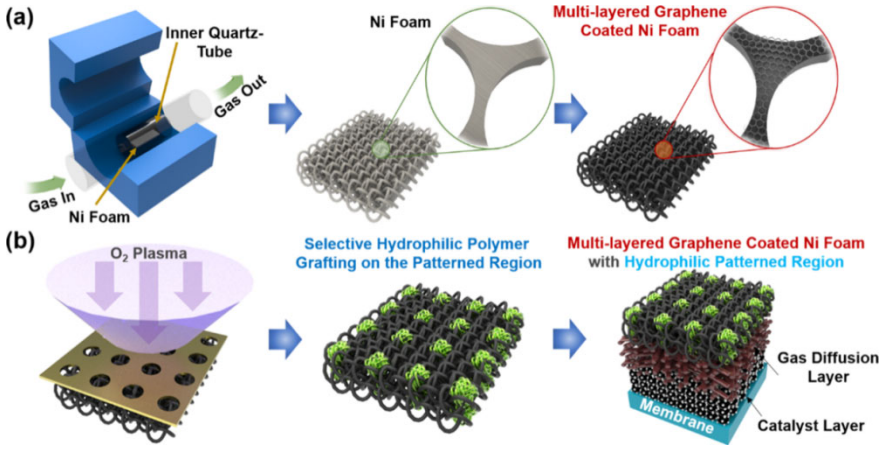


Figure 12. Schematic illustrations of preparation of MLG-coated Ni foam with patterned wettability: (**a**) growth of MLG on Ni foam, (**b**) selective grafting of hydrophilic polymer on MLG-coated Ni foam [208].

4.3. Three-Dimensional Metal Foam Flow Field

Porous metal materials combine the inherent advantages of the base material—such as electrical conductivity, thermal conductivity, and plasticity—with unique properties like porosity and specific surface area, enabling their widespread application in fluid distribution, heat transfer, and other fields. In PEMFCs, they were primarily used in the form of metal foam [209]. Metal foam flow channels offered superior water retention, more

uniform species distribution, and more uniform current density distribution. However, this flow field lacked a dominant flow direction and exhibited localized low-flow regions. More importantly, the pressure drop required for metal-foam-based flow channel designs was approximately three times that of parallel flow channel designs, posing challenges for reactant gas transport and water management in metal foam flow fields [210,211]. Consequently, many researchers have begun to focus on metal foam flow fields and investigate structural improvements.

Khatib et al. [212] used an open-pore cellular foam material to construct porous metal foam flow channels. The porous metal foam flow channels exhibited higher permeability, and the temperature and water management within the porous channels were superior to those of serpentine flow channels. Under the same operating conditions at 0.4 V, the fuel cell with porous flow channels outperformed the one with serpentine flow channels, achieving a 55% increase in current density. In addition, Zhang et al. [213] found that the current collection area on the GDL surface was significantly reduced in metal foam flow fields. However, due to the fine porous structure of the metal foam and the good physical contact formed with the GDL, the corresponding ohmic loss did not increase substantially. Compared with conventional channel-rib flow fields, metal foam flow fields could effectively make the internal distributions of oxygen and current density more uniform.

Figure 13 illustrates the metal foam flow field under low-relative-humidity and pressurized conditions. When foam materials were employed under low-humidity and pressurized conditions, water entrained in the gas and water produced by electrochemical reactions were stored within the pores. The fuel could utilize the residual water retained in the pores for humidification, thereby improving fuel cell performance [214]. Using X-ray scanning technology, Lv et al. [215] reconstructed the three-dimensional structure of the GDL and the metal foam flow field in a PEMFC. Compared with hydrophobic metal foam, a reasonably designed patterned wettability metal foam could significantly improve several performance aspects. These improvements include reducing the liquid water coverage at the foam interface, enhancing vertical gas convection within the GDL, and optimizing the pressure and gas velocity distributions in the metal foam flow field.

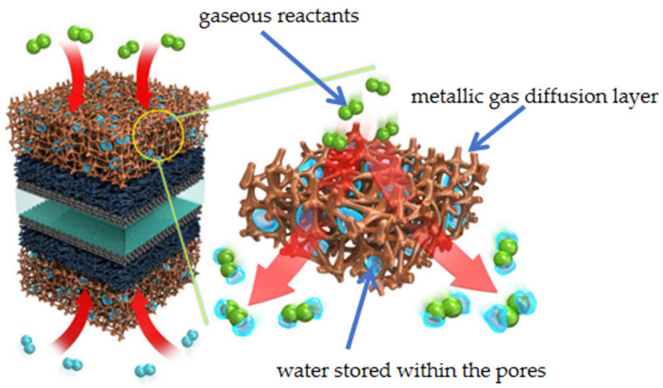


Figure 13. Schematic diagram of the metal foam flow field under low RH and pressurized conditions [214].

Porous metal foam materials have been proposed as alternative flow fields for PEMFCs, and their pore size or porosity level is an important factor affecting the performance of the metal foam flow field. In a uniform-pore-size metal foam flow field, reducing the pore size helped improve output performance and enhanced the uniformity of oxygen and current density distributions. The smaller the pore size, the higher the pores per inch (PPI), which means more pores per unit length and higher porosity of the material [216].

With the development of research, non-uniform pore size flow fields have gradually attracted researchers' attention, and their performance often surpasses that of uniform-

pore-size structures. Zhang et al. [217] found that, compared with parallel flow fields, the heat and mass transfer capabilities of metal foam flow fields were far superior to those of traditional parallel flow fields. When the porosity of the metal foam flow field decreased along the transverse flow channel direction, the fuel cell achieved better water management and more uniform reactant gas distribution. Tao et al. [218] proposed using a metal foam flow field with non-uniform pore size to improve the performance of large-area PEMFCs. By analyzing different pore size configurations, the results indicated that the best cell performance was achieved when the metal foam flow field had a pore size that decreased diagonally along the flow direction (from inlet to outlet).

The novel hierarchical pore structure of metal foam flow fields is also an extremely important and effective approach for optimizing pore architecture. Such a flow field increased the maximum net power density and water discharge capacity, and reduced the pressure drop. Sun et al. [219] designed a novel bilayer metal foam flow field using two different PPI values: 50 PPI for the first layer and 100 PPI for the second layer. Compared with conventional metal foams of 50 PPI and 110 PPI, this bilayer structure achieved significantly improved performance. Subsequently, Sun et al. [220] conducted numerical simulations on the water management characteristics and output performance of the novel metal foam flow field. The experimental results indicated that the water discharge capacity of the metal foam flow field with hierarchical pore structure was close to that of the parallel flow field. Meanwhile, it exceeded that of both the uniform coarse-pore metal foam flow field and the uniform fine-pore metal foam flow field.

4.4. Other Novel Three-Dimensional Flow Fields

Li et al. [221] designed and analyzed a novel three-dimensional flow field—a new wavy serpentine flow field. Its periodic wavy structure induced periodic variations in local flow direction, local velocity, and local pressure, thereby enhancing forced convection. Compared with the traditional serpentine flow field, the new wavy serpentine flow field exhibited a lower pressure drop across the entire current density range. It also improved cell performance in the high-current-density region, increasing the peak power density by 17.8%. Yin et al. [222] adopted an inversely phased wavy flow field design. Compared with the parallel wavy flow field, the inversely phased wavy flow field presented a unique membrane temperature distribution with multiple elliptical island-like patterns and achieved improved thermal uniformity and performance.

Unlike traditional linear channel flow fields, complex three-dimensional flow fields featured repetitively arranged baffles within the channels, which were referred to as baffle designs. These flow fields consequently induced microscale interfacial fluxes between the GDL and the flow field. The resulting high-intensity oxygen flow could remove excess water from the GDL, thereby improving fuel cell efficiency [223]. Cai et al. [224] proposed a novel 3D cathode flow field with main and sub-channels and a transition region, which included porous bottom ribs that facilitated uniform reactant distribution. This 3D flow field structure significantly enhanced the transport efficiency of reactants both in the flow direction and in the direction perpendicular to the flow. However, it also led to a slight increase in pressure drop and made the reactant distribution non-uniform. He et al. [225] designed a series of three-dimensional flow fields with trapezoidal baffles, which enhanced oxygen transport and water management capabilities.

3D flow field designs typically improve the performance of proton exchange membrane fuel cells, but the accompanying issue is a significant increase in pressure loss. To address this problem, Sun et al. [226] proposed a novel windward bend flow field. Compared with a cut cylindrical baffle channel and a 3D wavy channel, the windward bend flow channel featured a higher velocity component along the flow direction at the channel

and GDL interface. It exhibited excellent mass transfer performance and lower pressure loss under the constant extra power consumed by the auxiliary components of the fuel cell system.

5. Conclusions

The design of flow channels and flow fields was crucial for improving the power density and reducing costs of PEMFCs. Therefore, optimized flow channel designs and a range of novel flow fields have developed rapidly.

1. In parallel flow fields, longer channels benefited water management, and narrow channels suited high current densities. In serpentine flow fields, shorter paths improved current density uniformity, and reducing the channel-to-rib width ratio significantly enhances performance, but narrow channels increased pressure drop. In interdigitated flow fields, narrow outlet channels improved oxygen distribution and water removal, and the optimal channel aspect ratio was 1.00.

2. Flow fields with fewer channels generally featured better flow uniformity and cell performance. At a current density of 1000 mA/cm^2, the single-channel structure achieved 7% and 21% higher output performance than the dual-channel and four-channel structures, respectively, although it suffered a larger pressure drop.

3. Compared with rectangular and trapezoidal channels, the triangular channel offered the best cell performance, with stronger water management and oxygen transport capability. The rectangular channel provided a higher cell voltage and better overall electrical performance, while the trapezoidal channel cross-section was more favorable for reactant diffusion.

4. In terms of baffle selection, rectangular and trapezoidal baffles performed well under moderate blockage levels, and the former features higher output performance and current density. Triangular baffles are more suitable under high blockage or flooding-prone conditions.

5. Taller baffles and algorithm-optimized baffle height greatly boosted heat transfer and water removal efficiency. More baffles increased mass flux and improved the uniformity of reactant distribution but also raised the pressure drop. The optimal output performance occurred at a baffle angle of 45°.

6. The staggered arrangement was the most widely used and effective. The STBP flow field increased the maximum net power by 6.39% and 2.54% over the conventional parallel flow field and PTBP, respectively.

7. The parallel flow field had a low pressure drop but suffered from uneven gas distribution, flooding, and reactant starvation. The serpentine flow field improved water removal and mass transfer uniformity at the cost of high flow resistance and pressure drop. The interdigitated flow field offered excellent mass transfer and water drainage, yet its high resistance may damage the GDL. The composite flow field combined the advantages of multiple structures for synergistic performance optimization.

8. Tapered and wavy flow fields alter channel geometries along the flow path. The resultant accelerated flow enhanced oxygen delivery and water drainage. Among other novel flow fields, the pin-type flow field offered low pressure drop and good uniformity but was prone to stagnation zones and water accumulation; the spiral flow field enhanced heat and mass transfer through secondary vortices, demonstrating superior overall performance.

9. Bio-inspired flow fields, such as leaves, lungs, and trees, showed outstanding advantages in water management and stability. Nevertheless, their branched structures were prone to uneven distribution due to water blockage, and their performance was highly dependent on operating parameters. Among other novel flow fields, the spider-web-shaped flow field, characterized by polygonal outlines and spiral channels, achieved superior performance with a lower pressure drop. The bionic bamboo channels induced

flow disturbance to strengthen mass and heat transfer. The squid-fin bionic channels reduced flow resistance and pressure drop by retaining lateral flow spaces.

10. Self-humidifying structures effectively improved water management of PEMFCs. They enhanced cell performance and low-humidity adaptability through moisture retention and uniform water and heat distribution, facilitating the commercial application of fuel cells.

11. Three-dimensional fine-mesh flow fields could force repeated gas splitting, merging, and disturbance. This enhances oxygen concentration and distribution uniformity while suppressing flooding. 3D graphene foam flow fields used compressed graphene foam to form tortuous pores, accelerating reactant diffusion. 3D metal foam flow fields offered high porosity and uniform current density distribution, but caused considerable pressure loss and water accumulation. Currently, most research on 3D flow fields remains at the numerical simulation stage, leaving substantial room for improvement.

Future research directions for fuel cell flow fields include the following:

1. Flow channel geometric parameters directly determine fuel cell performance, and suitable channel dimensions should be designed for different operating conditions. Moderately increasing the baffle height and adopting a staggered arrangement could further optimize the baffle design. In addition, novel baffle structures should be actively explored and developed. The helical baffle induced forced convection and generated cross-flow beneath the ribs, thereby enhancing oxygen supply; the ship-type baffle enhanced mass transfer while producing relatively low extra power consumed by the auxiliary components of the fuel cell system.

2. To address the issue of liquid water blockage in existing leaf-shaped, lung-shaped, and tree-shaped bio-inspired flow fields, anti-clogging hierarchical multi-outlet bionic structures with gradient-width or variable-cross-section branch channels could be developed. Furthermore, more novel bio-inspired flow field designs should be continuously explored. For example, the bionic fish-scale porous flow field comprehensively reduced pressure drop, boosted water removal efficiency and optimized thermal performance simultaneously.

3. Traditional parallel, serpentine, and interdigitated flow fields have simple structures and low manufacturing costs. However, their inherent drawbacks are very obvious. Although composite, bionic, and three-dimensional flow fields ameliorated the deficiencies of traditional flow fields, they still suffered from complicated fabrication processes and high manufacturing costs. Therefore, future research should prioritize reducing the reliance on high-precision manufacturing techniques to promote the practical application of three-dimensional and other advanced flow fields.

4. A data-driven, model-based physics-informed neural network (PINN) to eliminate discrepancies between experimental measurements and numerical simulations is promising in the design and optimization of PEMFC flow fields. By embedding physical laws and incorporating experimental results, PINNs could effectively correct prediction errors. Reliable optimization of critical flow channel and baffle dimensions including channel width, depth, rib thickness, and baffle size could be achieved, thereby accelerating the development of high-performance PEMFC flow fields.

Author Contributions: Writing—Original Draft, Investigation, Project Administration, Visualization, Conceptualization, A.X.; Supervision, Project Administration, Conceptualization, Funding Acquisition, Writing—Review and Editing, S.Y.; Data Curation, Investigation, Methodology, Visualization, M.G.; Data Curation, Investigation, Visualization, H.D.; Data Curation, Investigation, Writing—Review and Editing, J.Z.; Investigation, Resources, Y.L.; Data Curation, Investigation, Y.Z.; Data Curation, Investigation, J.L.; Data Curation, Investigation, T.G.; Investigation, Resources, H.B. All authors have read and agreed to the published version of the manuscript.

Funding: This research was funded by the open fund project (general type) of the State Key Laboratory of Advanced Vehicle Integration and Control of China FAW group Co., Ltd. (GF-2024-02705); the Key Project of the Joint Fund for Regional Innovation and Development of the National Natural Science Foundation of China (Grant No. U25A20330); and the Department of Science and Technology of Jilin Province (Grant No. 20240301005ZD).

Data Availability Statement: No new data were created in this review article.

Acknowledgments: Gratitude was hereby expressed to Wiley, ACS Publications, World Scientific Connect and Nature Portfolio for granting copyright permission for the figures used in this work and to the Undergraduate Research Training Program of Jilin University for its support of this research.

Conflicts of Interest: Authors Yang Liu and Haidong Bian were employed by the company Faw Jiefang Automotive Company. The remaining authors declare that the research was conducted in the absence of any commercial or financial relationships that could be construed as a potential conflict of interest. The authors declare that this study received funding from Control of China FAW group Co., Ltd. The funder was not involved in the study design, collection, analysis, interpretation of data, the writing of this article or the decision to submit it for publication.

References

1. Jia, C.; Liu, W.; Chau, K.T.; He, H.; Zhou, J.; Niu, S. Passenger-aware reinforcement learning for efficient and robust energy management of fuel cell buses. *eTransportation* **2026**, *27*, 100537.
2. Lu, D.; Yi, F.; Hu, D.; Yang, Q.; Wang, J. Online optimization of energy management strategy for FCV control parameters considering dual power source lifespan decay synergy. *Appl. Energy* **2023**, *348*, 121516. [CrossRef]
3. Yi, F.; Shu, X.; Zhou, J.; Zhang, J.; Feng, C.; Gong, H.; Zhang, C.; Yu, W. Remaining useful life prediction of PEMFC based on matrix long short-term memory. *Int. J. Hydrogen Energy* **2025**, *111*, 228–237. [CrossRef]
4. Jia, C.; Liu, W.; He, H.; Chau, K.T. Decoupled safety supervision empowering efficient and safe energy management for fuel cell vehicles. *npj Sustain. Mobil. Transp.* **2026**, *3*, 16. [CrossRef]
5. Li, K.; Zhou, J.; Jia, C.; Yi, F.; Zhang, C. Energy sources durability energy management for fuel cell hybrid electric bus based on deep reinforcement learning considering future terrain information. *Int. J. Hydrogen Energy* **2024**, *52*, 821–833.
6. Wang, Y.; Liao, X.; Liu, G.; Xu, H.; Guan, C.; Wang, H.; Li, H.; He, W.; Qin, Y. Review of flow field designs for polymer electrolyte membrane fuel cells. *Energies* **2023**, *16*, 4207. [CrossRef]
7. Jia, C.; He, H.; Zhou, J.; Li, J.; Wei, Z.; Li, K. A novel health-aware deep reinforcement learning energy management for fuel cell bus incorporating offline high-quality experience. *Energy* **2023**, *282*, 128928.
8. Jia, C.; Liu, W.; He, H.; Chau, K.T. Superior energy management for fuel cell vehicles guided by improved DDPG algorithm: Integrating driving intention speed prediction and health-aware control. *Appl. Energy* **2025**, *394*, 126195. [CrossRef]
9. Hermann, A.; Chaudhuri, T.; Spagnol, P. Bipolar plates for PEM fuel cells: A review. *Int. J. Hydrogen Energy* **2005**, *30*, 1297–1302. [CrossRef]
10. Steele, B.C.H.; Heinzel, A. Materials for fuel-cell technologies. *Nature* **2001**, *414*, 345–352. [CrossRef] [PubMed]
11. Wang, J.; Wang, H. Discrete approach for flow field designs of parallel channel configurations in fuel cells. *Int. J. Hydrogen Energy* **2012**, *37*, 10881–10897. [CrossRef]
12. Xing, L.; Cai, Q.; Xu, C.; Liu, C.; Scott, K.; Yan, Y. Numerical study of the effect of relative humidity and stoichiometric flow ratio on PEM (proton exchange membrane) fuel cell performance with various channel lengths: An anode partial flooding modelling. *Energy* **2016**, *106*, 631–645. [CrossRef]
13. Bachman, J.; Charvet, M.; Santamaria, A.; Tang, H.Y.; Park, J.W.; Walker, R. Experimental investigation of the effect of channel length on performance and water accumulation in a PEMFC parallel flow field. *Int. J. Hydrogen Energy* **2012**, *37*, 17172–17179. [CrossRef]
14. Goebel, S.G. Impact of land width and channel span on fuel cell performance. *J. Power Sources* **2011**, *196*, 7550–7554. [CrossRef]
15. Scholta, J.; Escher, G.; Zhang, W.; Küppers, L.; Jörissen, L.; Lehnert, W. Investigation on the influence of channel geometries on PEMFC performance. *J. Power Sources* **2006**, *155*, 66–71. [CrossRef]
16. Lim, B.H.; Majlan, E.H.; Daud, W.R.W.; Rosli, M.I.; Husaini, T. Numerical analysis of modified parallel flow field designs for fuel cells. *Int. J. Hydrogen Energy* **2017**, *42*, 9210–9218. [CrossRef]
17. Manso, A.P.; Marzo, F.F.; Barranco, J.; Garikano, X.; Mujika, M.G. Influence of geometric parameters of the flow fields on the performance of a PEM fuel cell. A review. *Int. J. Hydrogen Energy* **2012**, *37*, 15256–15287. [CrossRef]
18. Xing, L.; Du, S.; Chen, R.; Mamlouk, M.; Scott, K. Anode partial flooding modelling of proton exchange membrane fuel cells: Model development and validation. *Energy* **2016**, *96*, 80–95. [CrossRef]

19. Wang, X.D.; Duan, Y.Y.; Yan, W.M.; Peng, X.F. Effects of flow channel geometry on cell performance for PEM fuel cells with parallel and interdigitated flow fields. *Electrochim. Acta* **2008**, *53*, 5334–5343. [CrossRef]
20. Shimpalee, S.; Greenway, S.; Van Zee, J.W. The impact of channel path length on PEMFC flow-field design. *J. Power Sources* **2006**, *160*, 398–406. [CrossRef]
21. Shimpalee, S.; Van Zee, J.W. Numerical studies on rib & channel dimension of flow-field on PEMFC performance. *Int. J. Hydrogen Energy* **2007**, *32*, 842–856. [CrossRef]
22. Ghanbarian, A.; Kermani, M.J.; Scholta, J.; Abdollahzadeh, M. Polymer electrolyte membrane fuel cell flow field design criteria–application to parallel serpentine flow patterns. *Energy Convers. Manag.* **2018**, *166*, 281–296.
23. Wang, X.D.; Duan, Y.Y.; Yan, W.M.; Peng, X.F. Local transport phenomena and cell performance of PEM fuel cells with various serpentine flow field designs. *J. Power Sources* **2008**, *175*, 397–407. [CrossRef]
24. Rocha, C.; Knöri, T.; Ribeirinha, P.; Gazdzicki, P. A review on flow field design for proton exchange membrane fuel cells: Challenges to increase the active area for MW applications. *Renew. Sustain. Energy Rev.* **2024**, *192*, 114198. [CrossRef]
25. Kerkoub, Y.; Benzaoui, A.; Haddad, F.; Ziari, Y.K. Channel to rib width ratio influence with various flow field designs on performance of PEM fuel cell. *Energy Convers. Manag.* **2018**, *174*, 260–275. [CrossRef]
26. Wang, C.; Zhang, Q.; Shen, S.; Yan, X.; Zhu, F.; Cheng, X.; Zhang, J. The respective effect of under-rib convection and pressure drop of flow fields on the performance of PEM fuel cells. *Sci. Rep.* **2017**, *7*, 43447. [CrossRef] [PubMed]
27. Manso, A.P.; Marzo, F.F.; Mujika, M.G.; Barranco, J.; Lorenzo, A. Numerical analysis of the influence of the channel cross-section aspect ratio on the performance of a PEM fuel cell with serpentine flow field design. *Int. J. Hydrogen Energy* **2011**, *36*, 6795–6808. [CrossRef]
28. Zhang, L.; Shi, Z. Optimization of serpentine flow field in proton-exchange membrane fuel cell under the effects of external factors. *Alex. Eng. J.* **2021**, *60*, 421–433. [CrossRef]
29. Zhang, X.; Chen, S.; Xia, Z.; Zhang, X.; Liu, H. Performance enhancements of PEM fuel cells with narrower outlet channels in interdigitated flow field. *Energy Procedia* **2019**, *158*, 1412–1417. [CrossRef]
30. Chen, S.; Xia, Z.; Zhang, X.; Wu, Y. Numerical studies of effect of interdigitated flow field outlet channel width on PEM fuel cell performance. *Energy Procedia* **2019**, *158*, 1678–1684. [CrossRef]
31. Bagherighajari, F.; Moradi Bilondi, A.; Abdollahzadehsangroudi, M.; Hamrang, A.; Páscoa, J.C. A parametric numerical study on the performance of polymer electrolyte membrane fuel cell with intermediate-blocked interdigitated flow field designs. *Fuel Cells* **2023**, *23*, 304–322. [CrossRef]
32. Abdulla, S.; Patnaikuni, V.S. Performance evaluation of Enhanced Cross flow Split Serpentine Flow Field design for higher active area PEM fuel cells. *Int. J. Hydrogen Energy* **2020**, *45*, 25970–25984. [CrossRef]
33. Limjeerajarus, N.; Charoen-Amornkitt, P. Effect of different flow field designs and number of channels on performance of a small PEFC. *Int. J. Hydrogen Energy* **2015**, *40*, 7144–7158. [CrossRef]
34. Liu, Z.; Li, Q.; Yang, S.; Zhang, H.; Chen, X.; Xie, N.; Deng, C.; Du, W. Numerical investigation of PEMFC performance based on different multistage serpentine flow field designs. *Chem. Eng. J.* **2024**, *500*, 156951. [CrossRef]
35. Zou, Y.; Hua, S.; Wu, H.; Chen, C.; Wei, Z.; Hu, Z.; Lei, Y.; Wang, J.; Zhou, D. Design of a new single-cell flow field based on the multi-physical coupling simulation for PEMFC durability. *Energies* **2023**, *16*, 5932.
36. Wu, Y.; Cho, J.I.S.; Neville, T.P.; Meyer, Q.; Ziesche, R.; Boillat, P.; Cochet, M.; Shearing, P.R.; Brett, D.J.L. Effect of serpentine flow-field design on the water management of polymer electrolyte fuel cells: An in-operando neutron radiography study. *J. Power Sources* **2018**, *399*, 254–263.
37. Mohammedi, A.; Sahli, Y.; Moussa, H.B. 3D investigation of the channel cross-section configuration effect on the power delivered by PEMFCs with straight channels. *Fuel* **2020**, *263*, 116713. [CrossRef]
38. Wang, X.D.; Lu, G.; Duan, Y.Y.; Lee, D.J. Numerical analysis on performances of polymer electrolyte membrane fuel cells with various cathode flow channel geometries. *Int. J. Hydrogen Energy* **2012**, *37*, 15778–15786. [CrossRef]
39. Kumar, A.; Reddy, R.G. Effect of channel dimensions and shape in the flow-field distributor on the performance of polymer electrolyte membrane fuel cells. *J. Power Sources* **2003**, *113*, 11–18. [CrossRef]
40. Li, C.; Xu, X.; Hu, H.; Mei, N.; Yang, Y. Numerical investigation into the effect of serpentine flow channel with a variable cross-section on the performance of proton exchange membrane fuel cell. *Int. J. Energy Res.* **2021**, *45*, 7719–7731.
41. Ahmed, D.H.; Sung, H.J. Effects of channel geometrical configuration and shoulder width on PEMFC performance at high current density. *J. Power Sources* **2006**, *162*, 327–339. [CrossRef]
42. Sayan, Y. Investigating the impact of inverted-trapezoidal cross-section flow channels on the performance of a proton exchange membrane fuel cell with a parallel flow channel configuration. *Renew. Energy* **2025**, *256*, 124001.
43. Liu, K.; Liu, Y.; Han, Q.; Pei, P.; Zhang, L.; Sun, H. Enhancing PEMFC performance through dome-like variable cross-section channels: A study on mass transfer and power density optimization. *Int. J. Electrochem. Sci.* **2025**, *20*, 100920.
44. Thapa, S.; Ganesh, V.; Agarwal, H.; Sahu, A.K. Performance evaluation of cathode channels with different cross-sections for open-cathode polymer electrolyte membrane fuel cell stack. *J. Power Sources* **2024**, *603*, 234398.

45. Xia, G.; Zhang, X.; Ma, D. Effects of baffle position in serpentine flow channel on the performance of proton exchange membrane fuel cells. *Chin. J. Chem. Eng.* **2024**, *69*, 250–262. [CrossRef]
46. Olukayode, N.; Qian, H.; Ye, S.; Hu, M.; Dai, Y.; Sui, S. Numerical investigation of the combined impact of flow channel's geometry and baffle blockage on the performance of proton exchange membrane fuel cells. *Int. J. Heat Mass Transf.* **2025**, *242*, 126885.
47. Wei, Y.; Feng, Y.; Zhao, J.; Li, J.; Li, H.; Tan, J. Numerical investigation of proton exchange membrane fuel cells with symmetrical serpentine channels equipped with baffles. *ACS Omega* **2025**, *10*, 1510–1518. [CrossRef] [PubMed]
48. Huang, Y.; Song, J.; Deng, X.; Chen, S.; Zhang, X.; Ma, Z.; Chen, L.; Wu, Y. Numerical investigation of baffle shape effects on performance and mass transfer of proton exchange membrane fuel cell. *Energy* **2023**, *266*, 126448.
49. Hong, W.; Li, Y.; Xie, F.; Liao, M. Design-oriented analysis of baffle structures for performance enhancement in proton exchange membrane fuel cells. *J. Power Sources* **2026**, *666*, 239155.
50. Perng, S.W.; Wu, H.W. A three-dimensional numerical investigation of trapezoid baffles effect on non-isothermal reactant transport and cell net power in a PEMFC. *Appl. Energy* **2015**, *143*, 81–95.
51. Belchor, P.M.; Forte, M.M.C.; Carpenter, D.E.O.S. Parallel serpentine-baffle flow field design for water management in a proton exchange membrane fuel cell. *Int. J. Hydrogen Energy* **2012**, *37*, 11904–11911. [CrossRef]
52. Wang, Y.; Guan, C.; Zhang, P.; Zhu, T.; Wang, S.; Zhu, Y.; Wang, X. Optimal design of a cathode flow field with a new arrangement of baffle plates for a high clean power generation of a polymer electrolyte membrane fuel cell. *J. Clean. Prod.* **2022**, *375*, 134187. [CrossRef]
53. Gao, T.; Deng, X.; Huang, Y.; Gong, L.; Peng, Y. Improved design and multi-objective optimization of parallel flow field in proton exchange membrane fuel cell. *Energy Convers. Manag.* **2025**, *345*, 120363. [CrossRef]
54. Ghasabehi, M.; Ghanbari, S.; Asadi, M.R.; Shams, M.; Kanani, H. Optimization of baffle and tapering integration in the PEM fuel cell flow field employing artificial intelligence. *Energy* **2024**, *302*, 131884. [CrossRef]
55. Ye, L.; Cheng, X.; Shi, Y.; Li, Z.; Ke, C.; He, Z.; Shi, A. Baffle structure effects on mass transfer and pressure drop of HT-PEMFC with orientated flow channels. *AIP Adv.* **2024**, *14*, 015003. [CrossRef]
56. Li, Z.; Wang, H.; Cheng, Y.; Zhang, K.; Zeng, K.; Zhang, C. Performance of the baffled flow-rate controlled external membrane humidifier for proton exchange membrane fuel cells. *Int. J. Therm. Sci.* **2025**, *218*, 110180. [CrossRef]
57. Cheng, T.; Liu, Q.; Jiang, G.; Zhao, Q.; Mu, D. The impact of baffle and taper channel tilt angle on the output performance of proton-exchange membrane fuel cells. *Fuel Cells* **2024**, *24*, 32–48.
58. Yin, Y.; Wu, S.; Qin, Y.; Otoo, O.N.; Zhang, J. Quantitative analysis of trapezoid baffle block sloping angles on oxygen transport and performance of proton exchange membrane fuel cell. *Appl. Energy* **2020**, *271*, 115257. [CrossRef]
59. Heidary, H.; Kermani, M.J.; Prasad, A.K.; Advani, S.G. Experimental and numerical studies of enhanced interdigitated flow field for PEM fuel cells. *J. Energy Eng.* **2021**, *147*, 04021026. [CrossRef]
60. Wang, X.; Qin, Y.; Wu, S.; Shangguan, X.; Zhang, J.; Yin, Y. Numerical and experimental investigation of baffle plate arrangement on proton exchange membrane fuel cell performance. *J. Power Sources* **2020**, *457*, 228034. [CrossRef]
61. Liu, Q.; Lan, F.; Chen, J.; Wang, J.; Zeng, C. Flow field structure design modification with helical baffle for proton exchange membrane fuel cell. *Energy Convers. Manag.* **2022**, *269*, 116175. [CrossRef]
62. Liu, Q.; Lan, F.; Wang, J.; Chen, Y.; Chen, J. Multi-objective optimization of helical baffle flow field structure for fuel cell under multiple performance indicator constraints. *Renew. Energy* **2025**, *241*, 122349. [CrossRef]
63. Cai, Y.; Yue, S.; Wei, F.; Hu, J.; Chen, B. Research on performance of proton exchange membrane fuel cell with an innovative flow field. *Case Stud. Therm. Eng.* **2023**, *50*, 103418. [CrossRef]
64. Yang, H.; Cheng, T.; Mao, Y. Design and optimization of water drop curve baffles in high temperature PEMFC channel. *Ionics* **2024**, *30*, 8221–8232. [CrossRef]
65. Zhao, Z.; He, W.; Guo, B.; Wang, Z.; Qin, X. Advanced flow field design for fuel cells based on aerodynamic profile baffle structures. *Int. J. Hydrogen Energy* **2025**, *186*, 152036. [CrossRef]
66. Zhang, X.; Yang, X.; Gao, W.; Wang, C. An experimental research on the net output power and current density distribution of PEM fuel cells with trapezoid baffled flow fields. *Int. J. Energy Res.* **2021**, *45*, 21464–21475. [CrossRef]
67. Deng, X.; Zhang, E.; Lei, J.; Jia, D.; Liu, Y.; Shuchao, H.E. Numerical study on the effect of an improved three-partition baffle flow field on proton exchange membrane fuel cell performance. *ACS Omega* **2022**, *7*, 42872–42882. [CrossRef] [PubMed]
68. Fahruddin, A.; Ichsani, D.; Taufany, F.; Widodo, B.U.; Widodo, W.A. The effect of baffle shape on the performance of a polymer electrolyte membrane fuel cell with a biometric flow field. *Int. J. Hydrogen Energy* **2021**, *46*, 6028–6036. [CrossRef]
69. Xia, L.; Yu, Z.; Xu, G.; Ji, S.; Sun, B. Design and optimization of a novel composite bionic flow field structure using three-dimensional multiphase computational fluid dynamic method for proton exchange membrane fuel cell. *Energy Convers. Manag.* **2021**, *247*, 114707. [CrossRef]
70. Zhou, Y.; Chen, B. Investigation of optimization and evaluation criteria for flow field in proton exchange membrane fuel cell: A critical review. *Renew. Sustain. Energy Rev.* **2023**, *185*, 113584. [CrossRef]

71. Marappan, M.; Palaniswamy, K.; Velumani, T.; Chul, K.B.; Velayutham, R.; Shivakumar, P.; Sundaram, S. Performance studies of proton exchange membrane fuel cells with different flow field designs–review. *Chem. Rec.* **2021**, *21*, 663–714. [PubMed]
72. Feser, J.P.; Prasad, A.K.; Advani, S.G. On the relative influence of convection in serpentine flow fields of PEM fuel cells. *J. Power Sources* **2006**, *161*, 404–412. [CrossRef]
73. Wang, X.D.; Zhang, X.X.; Yan, W.M.; Lee, D.J.; Su, A. Determination of the optimal active area for proton exchange membrane fuel cells with parallel, interdigitated or serpentine designs. *Int. J. Hydrogen Energy* **2009**, *34*, 3823–3832. [CrossRef]
74. Rimon, S.T.A.; Shajid, S.R.; Mourshed, M.; Tushar, M.S.H.K. Flow field configurations in PEMFCs: Design, Modeling, and performance insights. *Energy Convers. Manag. X* **2025**, *28*, 101263. [CrossRef]
75. Pellegri, A.; Spaziante, P.M. Bipolar Separator for Electrochemical Cells and Method of Preparation Thereof. U.S. Patent 4,197,178, 8 April 1980.
76. Chakraborty, S.; Elangovan, D.; Palaniswamy, K.; Fly, A.; Ravi, D.; Seelan, D.A.S.; Rajagopal, T.K.R. A review on the numerical studies on the performance of proton exchange membrane fuel cell (PEMFC) flow channel designs for automotive applications. *Energies* **2022**, *15*, 9520. [CrossRef]
77. Chen, G.; Shi, W.; Xuan, J.; Penga, Ž.; Xu, Q.; Guo, H.; Su, H.; Xing, L. Improvement of under-the-rib oxygen concentration and water removal in proton exchange membrane fuel cells through three-dimensional metal printed novel flow fields. *AIChE J.* **2022**, *68*, e17758.
78. Wang, Y.; Wang, X.; Chen, G.; Chen, C.; Wang, X.; Penga, Ž.; Yang, Z.; Xing, L. Reinforcement of proton-exchange membrane fuel cell performance through a novel flow field design with auxiliary channels and a hole array. *AIChE J.* **2022**, *68*, e17461.
79. Wang, G.; Wang, H.; Jiang, L.; Lin, P.; Li, J.; Sun, J. Numerical study on dual-region mass transport at wave flow field of proton exchange membrane fuel cell. *Fuel Cells* **2022**, *22*, 12–22.
80. Tian, C.; Yuan, F.; Deng, T.; He, Q.; Hu, C.; Chen, Y.; Liu, W. Coupled optimization of auxiliary channels and porosity gradient of GDL for PEMFC. *Energy* **2024**, *301*, 131734. [CrossRef]
81. Fu, H.; Wang, R.; Li, Z. Comprehensive numerical study of baffle integration, channel arrangements, and a novel dual-stepped-U flow field for PEM fuel cells. *Int. J. Hydrogen Energy* **2025**, *189*, 151982.
82. Velisala, V.; Srinivasulu, G.N. Numerical simulation and experimental comparison of single, double and triple serpentine flow channel configuration on performance of a PEM fuel cell. *Arab. J. Sci. Eng.* **2018**, *43*, 1225–1234.
83. Qi, Z.; Kaufman, A. PEM fuel cell stacks operated under dry-reactant conditions. *J. Power Sources* **2002**, *109*, 469–476. [CrossRef]
84. Babay, M.A.; Adar, M.; Chebak, A.; Mabrouki, M. Exploring the sustainability of serpentine flow-field fuel cell, straight channel PEM fuel cells hight temperature through numerical analysis. *Energy Nexus* **2024**, *14*, 100283. [CrossRef]
85. Enearu, O.L.; Chen, Y.K.; Kalyvas, C.; Chukwu, O.D. A Simulation Study of PEMFC Flow Channels Using a New Hybrid Method. In *Innovative Techniques and Applications of Modelling, Identification and Control: Selected and Expanded Reports from ICMIC'17*; Springer: Berlin/Heidelberg, Germany, 2018; pp. 345–356.
86. Dong, P.; Jia, Y.; Xie, G.; Ni, M. The energy performance improvement of a PEM fuel cell with various chaotic flowing channels. *Int. J. Energy Res.* **2019**, *43*, 5460–5478. [CrossRef]
87. Kaiser, R.; Ahn, C.Y.; Lee, S.Y.; Kim, Y.H.; Park, J.C. Numerical analysis of water management and reactant distribution in PEM fuel cells with a convergent 5-channel serpentine flow field for emission-free ships. *Int. J. Nav. Archit. Ocean Eng.* **2025**, *17*, 100649. [CrossRef]
88. Zuo, Q.; Wang, G.; Shen, Z.; Ma, Y.; Ouyang, Y.; Yang, D.; Lei, S.; Ouyang, M. Performance evaluation and field synergy analysis of PEMFC with novel snake coil flow field. *Int. J. Heat Mass Transf.* **2025**, *238*, 126470.
89. Boni, M.; Velisala, V.; Sudi, V.S.S.; Adarsh Kumar, M. Performance analysis of proton exchange membrane fuel cells with various serpentine flow channel designs. *Environ. Prog. Sustain. Energy* **2025**, *44*, e14627. [CrossRef]
90. Suresh, P.V.; Jayanti, S.; Deshpande, A.P.; Haridoss, P. An improved serpentine flow field with enhanced cross-flow for fuel cell applications. *Int. J. Hydrogen Energy* **2011**, *36*, 6067–6072. [CrossRef]
91. Abdulla, S.; Patnaikuni, V.S. Enhanced cross-flow split serpentine flow field design for square cross-sectional polymer electrolyte membrane fuel cell. *Electrochim. Acta* **2021**, *391*, 138884.
92. Duc, T.V.; Ba, H.N.; Kim, H.C. Enhanced uniformity of reactants and water content in single-and multi-serpentine channel of proton-exchange membrane fuel cell. *Renew. Energy* **2025**, *247*, 123049.
93. Saminathan, J.; Marappan, M.; Angappamudaliar Palanisamy, S.K.; Ramasamy, S. Performance improvement of proton exchange membrane fuel cell by modified flow field design. *J. Energy Eng.* **2023**, *149*, 04023034. [CrossRef]
94. Zhang, S.; Ren, H.; Fang, H.; Zhang, Y.; Liu, Q. Design of flow field structure and three-dimensional multiphase flow simulation for bipolar plates in the proton exchange membrane fuel cell: A novel bio-inspired conjugate dual-channel serpentine flow path. *Fuel* **2026**, *405*, 136675.
95. Wang, J. Theory and practice of flow field designs for fuel cell scaling-up: A critical review. *Appl. Energy* **2015**, *157*, 640–663. [CrossRef]

96. He, W.; Yi, J.S.; Van Nguyen, T. Two-phase flow model of the cathode of PEM fuel cells using interdigitated flow fields. *AIChE J.* **2000**, *46*, 2053–2064.
97. Yan, W.M.; Mei, S.C.; Soong, C.Y.; Liu, Z.S.; Song, D. Experimental study on the performance of PEM fuel cells with interdigitated flow channels. *J. Power Sources* **2006**, *160*, 116–122. [CrossRef]
98. Hu, G.; Fan, J.; Chen, S.; Liu, Y.; Cen, K. Three-dimensional numerical analysis of proton exchange membrane fuel cells (PEMFCs) with conventional and interdigitated flow fields. *J. Power Sources* **2004**, *136*, 1–9. [CrossRef]
99. Wang, L.; Liu, H. Performance studies of PEM fuel cells with interdigitated flow fields. *J. Power Sources* **2004**, *134*, 185–196. [CrossRef]
100. Hu, P.; Peng, L.; Zhang, W.; Lai, X. Optimization design of slotted-interdigitated channel for stamped thin metal bipolar plate in proton exchange membrane fuel cell. *J. Power Sources* **2009**, *187*, 407–414. [CrossRef]
101. Bhattarai, A.; Wai, N.; Schweiss, R.; Whitehead, A.; Scherer, G.G.; Ghimire, P.C.; Lim, T.M.; Hng, H.H. Vanadium redox flow battery with slotted porous electrodes and automatic rebalancing demonstrated on a 1 kW system level. *Appl. Energy* **2019**, *236*, 437–443. [CrossRef]
102. Mohammadtabar, N.; Bakhshi-Jooybari, M.; Hosseinipour, S.J.; Gorji, A.H. Feasibility study of a double-step hydroforming process for fabrication of fuel cell bipolar plates with slotted interdigitated serpentine flow field. *Int. J. Adv. Manuf. Technol.* **2016**, *85*, 765–777.
103. Peng, L.; Mai, J.; Hu, P.; Lai, X.; Lin, Z. Optimum design of the slotted-interdigitated channels flow field for proton exchange membrane fuel cells with consideration of the gas diffusion layer intrusion. *Renew. Energy* **2011**, *36*, 1413–1420. [CrossRef]
104. Peng, L.; Lai, X.; Yi, P.; Mai, J.; Ni, J. Design, optimization, and fabrication of slotted-interdigitated thin metallic bipolar plates for PEM fuel cells. *J. Fuel Cell Sci. Technol.* **2011**, *8*, 011002.
105. Moslemi, M.; Javaherdeh, K.; Ashorynejad, H.R. Effect of compression of microporous and gas diffusion layers on liquid water transport of PEMFC with interdigitated flow field by Lattice Boltzmann method. *Colloids Surf. A Physicochem. Eng. Asp.* **2022**, *642*, 128623. [CrossRef]
106. Deng, S.; Hao, M.; Wang, R.; Zhang, J.; Zhang, X.; Li, Y. Improving water retention and mass transport for low-humidity proton exchange membrane fuel cells via a porous-channel interdigitated flow field. *Int. J. Hydrogen Energy* **2024**, *95*, 874–887.
107. Asadi, M.R.; Ghasabehi, M.; Ghanbari, S.; Shams, M. The optimization of an innovative interdigitated flow field proton exchange membrane fuel cell by using artificial intelligence. *Energy* **2024**, *290*, 130131.
108. Hamrang, A.; Abdollahzadeh, M.; Kermani, M.J.; Rahgoshay, S.M. Numerical simulation of the PEM fuel cell performance enhancement by various blockage arrangement of the cathode serpentine gas flow channel outlets/inlets. *Int. J. Heat Mass Transf.* **2022**, *186*, 122475. [CrossRef]
109. Fan, F.; Gu, M.; Chen, Y.; Zhang, D.; Fang, H.; Hu, B.; Zhang, Y.; Liu, Q. Comprehensive performance investigation of the novel mixed flow field for proton exchange membrane fuel cells: Three-dimensional multiphase simulation of a full-scale cell. *Chem. Eng. Process.-Process Intensif.* **2025**, *211*, 110234.
110. Gao, T.; Huang, Y.; Yan, J.; Zhang, X.; Ma, Z. Numerical simulation analysis of composite flow field design on mass transfer in proton exchange membrane fuel cell. *Int. J. Heat Mass Transf.* **2024**, *232*, 125956. [CrossRef]
111. Sevinc, H. Numerical investigation of a hybrid serpentine–pin flow field for enhanced PEMFC performance under variable operating conditions. *Eng. Sci. Technol. Int. J.* **2026**, *77*, 102338. [CrossRef]
112. Makkus, R.C.; Janssen, A.H.H.; de Bruijn, F.A.; Mallant, R.K. Stainless steel for cost-competitive bipolar plates in PEMFCs. *Fuel Cells Bull.* **2000**, *3*, 5–9. [CrossRef]
113. Tawfik, H.; Hung, Y.; Mahajan, D. Metal bipolar plates for PEM fuel cell—A review. *J. Power Sources* **2007**, *163*, 755–767. [CrossRef]
114. Wu, S.; Tongsh, C.; Du, Q.; Park, J.W.; Jiao, K. A comprehensive experimental investigation of the operating conditions on the performance of proton exchange membrane fuel cell using metal foam as cathode flow field. *Int. J. Green Energy* **2025**, *22*, 1886–1898.
115. Awin, Y.; Dukhan, N. Experimental performance assessment of metal-foam flow fields for proton exchange membrane fuel cells. *Appl. Energy* **2019**, *252*, 113458. [CrossRef]
116. Makkus, R.C.; Janssen, A.H.H.; de Bruijn, F.A.; Mallant, R.K. Use of stainless steel for cost competitive bipolar plates in the SPFC. *J. Power Sources* **2000**, *86*, 274–282. [CrossRef]
117. Wang, H.; Turner, J.A. Ferritic stainless steels as bipolar plate material for polymer electrolyte membrane fuel cells. *J. Power Sources* **2004**, *128*, 193–200. [CrossRef]
118. Tanaka, S.; Shudo, T. Corrugated mesh flow channel and novel microporous layers for reducing flooding and resistance in gas diffusion layer-less polymer electrolyte fuel cells. *J. Power Sources* **2014**, *268*, 183–193. [CrossRef]
119. Gao, W.; Li, Q.; Sun, K.; Chen, R.; Che, Z.; Wang, T. Mass transfer and water management in proton exchange membrane fuel cells with a composite foam-rib flow field. *Int. J. Heat Mass Transf.* **2023**, *216*, 124595. [CrossRef]
120. Li, Q.; Suo, M.; Sun, K.; Tao, X.; Zeng, Z.; Liu, H.; Che, Z.; Wang, T. Experimental study on the performance of proton exchange membrane fuel cell with foam/channel composite flow fields. *J. Power Sources* **2024**, *620*, 235244. [CrossRef]

121. Kim, J.; Kim, J. Enhanced mass transport in polymer electrolyte membrane fuel cell using hybrid metal-foam/serpentine flow field. *J. Appl. Electrochem.* **2026**, *56*, 60.
122. Wang, B.; Pan, W.; Hu, Z.; Tang, L.; Chen, X.; Wang, F. Metal Foam-Leaf Vein Stratified Flow Field for Enhanced Performance of Proton Exchange Membrane Fuel Cells. *Energy Technol.* **2026**, *14*, e202501750.
123. Wu, Y.; Xu, L.; Zhou, S.; Yang, J.; Kockelmann, W.; Han, Y.; Li, Q.; Chen, W.; Coppens, M.O.; Shearing, P.R.; et al. Water management and mass transport of a fractal metal foam flow-field based polymer electrolyte fuel cell using operando neutron imaging. *Appl. Energy* **2024**, *364*, 123204. [CrossRef]
124. Ghasabehi, M.; Ashrafi, M.; Shams, M. Performance analysis of an innovative parallel flow field design of proton exchange membrane fuel cells using multiphysics simulation. *Fuel* **2021**, *285*, 119194. [CrossRef]
125. Timurkutluk, B.; Chowdhury, M.Z. Numerical investigation of convergent and divergent parallel flow fields for PEMFCs. *Fuel Cells* **2018**, *18*, 441–448. [CrossRef]
126. Huang, H.; Liu, M.; Li, X.; Guo, X.; Wang, T.; Li, S.; Lei, H. Numerical simulation and visualization study of a new tapered-slope serpentine flow field in proton exchange membrane fuel cell. *Energy* **2022**, *246*, 123406. [CrossRef]
127. Chowdhury, M.Z.; Akansu, Y.E. Novel convergent-divergent serpentine flow fields effect on PEM fuel cell performance. *Int. J. Hydrogen Energy* **2017**, *42*, 25686–25694. [CrossRef]
128. Chowdhury, M.Z.; Timurkutluk, B. Transport phenomena of convergent and divergent serpentine flow fields for PEMFC. *Energy* **2018**, *161*, 104–117. [CrossRef]
129. Kuo, J.K. Evaluating the enhanced performance of a novel wave-like form gas flow channel in the PEMFC using the field synergy principle. *J. Power Sources* **2006**, *162*, 1122–1129. [CrossRef]
130. Li, M.; Fu, L.; Lin, H.; Liu, J.; Zhang, X. Wave flow field design optimization for enhanced performance of high-temperature PEM fuel cells. *Fuel* **2026**, *406*, 137136.
131. Ding, Q.; Zhao, H.L.; Wan, Z.M.; Yang, Y.R.; Yang, C.; Wang, X.D. Performance of parallel, interdigitated, and serpentine flow field PEM fuel cells with straight or wavelike channels. *J. Energy Eng.* **2020**, *146*, 04020054. [CrossRef]
132. Seyhan, M.; Akansu, Y.E.; Murat, M.; Korkmaz, Y.; Akansu, S.O. Performance prediction of PEM fuel cell with wavy serpentine flow channel by using artificial neural network. *Int. J. Hydrogen Energy* **2017**, *42*, 25619–25629. [CrossRef]
133. Chen, L.; Lou, M.; Lu, K.; Zhao, Z.; Lin, R. Optimizing Under-Rib Mass Transfer to Regulate Water–Gas Distribution in Proton Exchange Membrane Fuel Cells for Performance Enhancement across Wide-Range Humidity. *J. Phys. Chem. C* **2025**, *129*, 12750–12761.
134. Wang, B.; Pan, W.; Hu, Z.; Zhang, G.; Tang, L.; Chen, X.; Wang, F. Impacts of scale-up and flow uniformity on performance of PEM fuel cells with wave flow fields. *Renew. Energy* **2025**, *255*, 123691. [CrossRef]
135. Wang, H.; Fang, H.; Guo, J.; Lin, Y. Design and optimization of variable cross-section wave flow channels in proton exchange membrane fuel cells based on physical field. *Int. J. Green Energy* **2026**, *23*, 599–617.
136. Wen, D.-H.; Yin, L.-Z.; Piao, Z.-Y.; Lu, C.-D.; Li, G.; Leng, Q.-H. A novel intersectant flow field of metal bipolar plate for proton exchange membrane fuel cell. *Int. J. Energy Res.* **2017**, *41*, 2184–2193. [CrossRef]
137. Ma, Q.; Li, X.; Zhao, P.; Wang, H.; Du, W.; Liu, F.; Zheng, L.; He, Y. Optimization design on the rhombic flow field of bipolar plate for proton exchange membrane fuel cells. *Ionics* **2025**, *31*, 13053–13066. [CrossRef]
138. Li, Y.; Wilberforce, T.; Li, J. Flow channel optimization for proton exchange membrane fuel cell using zig-zag geometry. *Int. J. Hydrogen Energy* **2025**, *142*, 1140–1152. [CrossRef]
139. Zaffora, A.; Barbera, O.; Gallo, E.; Santamaria, M.; Giacoppo, G. The effect of pin-type flow field plate design on the current distribution in a H2-fed polymer electrolyte fuel cell. *J. Power Sources* **2024**, *616*, 235129.
140. Dang, D.K.; Zhou, B. Flow Dynamics, Liquid Water Flooding and Removal Characteristics in a PEMFC Cathode with Hexagon-Pin Flow Field. *Automot. Innov.* **2025**, *8*, 472–485. [CrossRef]
141. Tan, J.; Zhang, B.; Xing, P.; Liu, Q.; Yu, Z.; Gong, Y.; Ma, X. Numerical modelling and performance study of an anion-exchange membrane electrolyzer with spiral flow channel. *Int. J. Hydrogen Energy* **2025**, *179*, 151679. [CrossRef]
142. Jang, J.Y.; Cheng, C.H.; Liao, W.T.; Huang, Y.X.; Tsai, Y.C. Experimental and numerical study of proton exchange membrane fuel cell with spiral flow channels. *Appl. Energy* **2012**, *99*, 67–79. [CrossRef]
143. Yao, J.; Yan, F.; Pei, X. CFD Analysis of Spiral Flow Fields in Proton Exchange Membrane Fuel Cells. *Fluid Dyn. Mater. Process.* **2023**, *19*, 1425. [CrossRef]
144. Zheng, T.; Meng, F.; Fan, W.; Liu, M.; Lu, D.; Luan, Y.; Su, X.; Lu, G.; Liu, Z. AI-assisted flow field design for proton exchange membrane fuel cells: Progress and perspective. *J. Bionic Eng.* **2025**, *22*, 47–64.
145. Wang, Z.; Yang, J.; Wang, H.; Xiao, N.; Li, A.; Wang, R.; Ming, W. Biomimetic structures for water management in proton exchange membrane fuel cells: A review. *Int. J. Electrochem. Sci.* **2026**, *21*, 101319. [CrossRef]
146. Kloess, J.P.; Wang, X.; Liu, J.; Shi, Z.; Guessous, L. Investigation of bio-inspired flow channel designs for bipolar plates in proton exchange membrane fuel cells. *J. Power Sources* **2009**, *188*, 132–140. [CrossRef]

147. Kang, H.C.; Jum, K.M.; Sohn, Y.J. Performance of unit PEM fuel cells with a leaf-vein-simulating flow field-patterned bipolar plate. *Int. J. Hydrogen Energy* **2019**, *44*, 24036–24042.
148. Dong, J.; Liu, S.; Liu, S. Numerical investigation of novel bio-inspired flow field design scheme for PEM fuel cell. *J. Renew. Sustain. Energy* **2020**, *12*, 044303. [CrossRef]
149. Xiao, F.; Chen, T.; Lan, Y.; Chen, Z. Flow field design and parameter optimization of PEMFC based on leaf vein structure. *Renew. Energy* **2025**, *241*, 122317.
150. Huang, Z.; Chen, Y.; Wu, W.; Li, M.; Liu, X.; Rao, Z. A novel leaf bionic flow field with structured multi-level channel based on Murray's law in proton exchange membrane fuel cell for enhanced mass transfer. *Phys. Fluids* **2024**, *36*, 113617.
151. Zhu, H.; Ma, Y.; Zhang, L.; Liu, H. Multi-objective optimization of proton exchange membrane fuel cell performance based on a new leaf-shaped flow field. *Int. J. Hydrogen Energy* **2025**, *120*, 254–275.
152. Ghadhban, S.A.; Alawee, W.H.; Dhahad, H.A. Study effects of bio-inspired flow filed design on Polymer Electrolyte Membrane fuel cell performance. *Case Stud. Therm. Eng.* **2021**, *24*, 100841. [CrossRef]
153. Wang, H.; Chang, K.; Yang, J.; Luo, Z.; Cheng, Q. Multi-objective optimization of bionic leaf-vein flow field for a PEMEC based on neural network and genetic algorithm. *Int. J. Hydrogen Energy* **2025**, *100*, 1083–1094.
154. Fahruddin, A.; Ichsani, D.; Taufany, F.; Widodo, B.U.K. The effect of mother channel width on biometric flow field towards polymer electrolyte membrane fuel cell performance. *J. Phys. Conf. Ser.* **2019**, *1402*, 044042. [CrossRef]
155. Lian, Y.; Xie, Q.; Zheng, M. Investigation on the optimal angle of a flow-field design based on the leaf-vein structure for PEMFC. *J. New Mater. Electrochem. Syst.* **2020**, *23*, 262–268.
156. Muñoz-Perales, V.; Van der Heijden, M.; García-Salaberri, P.A.; Vera, M.; Forner-Cuenca, A. Engineering lung-inspired flow field geometries for electrochemical flow cells with stereolithography 3d printing. *ACS Sustain. Chem. Eng.* **2023**, *11*, 12243–12255. [CrossRef] [PubMed]
157. Bethapudi, V.S.; Hack, J.; Hinds, G.; Shearing, P.R.; Brett, D.J.L.; Coppens, M.O. Electro-thermal mapping of polymer electrolyte membrane fuel cells with a fractal flow-field. *Energy Convers. Manag.* **2021**, *250*, 114924. [CrossRef]
158. Ghanbari, S.; Ghasabehi, M.; Asadi, M.R.; Shams, M. An inquiry into transport phenomena and artificial intelligence-based optimization of a novel bio-inspired flow field for proton exchange membrane fuel cells. *Appl. Energy* **2024**, *376*, 124260.
159. Xie, Y.; Huang, Y.; Zeng, J.; Gao, T.; Ye, D.; Chai, R. Enhanced performance of PEMFC through novel flow field design and optimization. *Int. J. Heat Mass Transf.* **2026**, *255*, 127792.
160. Lu, G.; Fan, W.; Lu, D.; Zhao, T.; Wu, Q.; Liu, M.; Liu, Z. Lung-inspired hybrid flow field to enhance PEMFC performance: A case of dual optimization by response surface and artificial intelligence. *Appl. Energy* **2024**, *355*, 122255.
161. Stephenson, D.; Patronis, A.; Holland, D.M.; Lockerby, D.A. Generalizing Murray's law: An optimization principle for fluidic networks of arbitrary shape and scale. *J. Appl. Phys.* **2015**, *118*, 174302.
162. Wan, X.; Cao, J.; Yang, X.; Wang, L.; Chen, Y.; Cheng, B. Research on the flow field of the PEMFC bipolar plate based on the tree-like fractal theory. *Fractals* **2023**, *31*, 2340185. [CrossRef]
163. Tan, Q.; Lei, H.; Liu, Z. Numerical simulation analysis of the performance on the PEMFC with a new flow field designed based on constructal-theory. *Int. J. Hydrogen Energy* **2022**, *47*, 11975–11990. [CrossRef]
164. Liu, H.; Wen, Q.; Ji, L.; Yin, K.; He, S.; Cao, J.; Xiao, Y. Effect of New Fractal Flow Field Structure on the Performance of Hydrogen Fuel Cell. *Fractals* **2025**, *33*, 1–11. [CrossRef]
165. Lorenzini-Gutierrez, D.; Hernandez-Guerrero, A.; Ramos-Alvarado, B.; Perez-Raya, I.; Alatorre-Ordaz, A. Performance analysis of a proton exchange membrane fuel cell using tree-shaped designs for flow distribution. *Int. J. Hydrogen Energy* **2013**, *38*, 14750–14763. [CrossRef]
166. Damian-Ascencio, C.E.; Saldaña-Robles, A.; Hernandez-Guerrero, A.; Cano-Andrade, S. Numerical modeling of a proton exchange membrane fuel cell with tree-like flow field channels based on an entropy generation analysis. *Energy* **2017**, *133*, 306–316. [CrossRef]
167. Chen, X.; Chai, F.; Hu, S.; Tan, J.; Luo, L.; Xie, H.; Wan, Z.; Qu, Z. Design of PEMFC bipolar plate cooling flow field based on fractal theory. *Energy Convers. Manag. X* **2023**, *20*, 100445. [CrossRef]
168. Jiang, S.; Zhai, C.; Wang, B.; Zhang, F.; Wang, Z.; Han, J.; Jiao, K. Review on Self-Humidifying Fuel Cell Systems: Materials, Systems, and Challenges. *Electrochem. Energy Rev.* **2026**, *9*, 11. [CrossRef]
169. Lian, Y.; You, C.; Zhu, Z.; Zhu, X.; Li, X.; Zhou, W. Preparation and performance of a self-humidifying fuel cell using a fiber sintered sheet as flow field. *J. Power Sources* **2022**, *536*, 231513. [CrossRef]
170. Lian, Y.; Zhu, Z.; You, C.; Lin, L.; Lin, F.; Lin, L.; Huang, Y.; Zhou, W. Structural optimization of fiber porous self-humidifying flow field plates applied to proton exchange membrane fuel cells. *Energy* **2023**, *271*, 127034. [CrossRef]
171. Qiao, K.; Liu, H.; Huang, S.; Zeng, X.; Cao, D. Designing self-humidifying proton exchange membrane fuel cells by using patterned acid-alkaline hybrid cathodes. *Int. J. Hydrogen Energy* **2024**, *50*, 209–220.
172. Wang, Y.; Zhang, W.; Liu, H.; Xu, Q.; Khotseng, L.; Cheng, Y.; Su, H. Cultivating titanium dioxide nanoarrays on gas diffusion layer for advancing self-humidifying proton exchange membrane fuel cell. *Fuel* **2024**, *366*, 131322. [CrossRef]

173. Tong, G.; Xu, X.; Yuan, Q.; Yang, Y.; Tang, W.; Sun, X. Simulation study of proton exchange membrane fuel cell cross-convection self-humidifying flow channel. *Int. J. Energy Res.* **2021**, *45*, 4036–4047.
174. Maia, L.K.K.; Sousa, R., Jr. Three-dimensional CFD modeling of direct ethanol fuel cells: Evaluation of anodic flow field structures. *J. Appl. Electrochem.* **2017**, *47*, 25–37.
175. Wang, J.; Wang, H. Flow-field designs of bipolar plates in PEM fuel cells: Theory and applications. *Fuel Cells* **2012**, *12*, 989–1003.
176. Liang, H.; Zhang, P.; Bu, W.; Gu, W.; Zheng, M.; Zhu, W.; Wang, B. Data analysis of a five-inlet radial flow field bipolar plate for enhanced mass transport in PEMFC Applications. *Fuel* **2026**, *405*, 136624.
177. Dang, D.K.; Zhou, B. Investigation of liquid water behaviors inside a PEMFC cathode with a leaf-like biomimetic flow field design based on Murray's Law. *Int. J. Green Energy* **2022**, *19*, 577–591.
178. Dang, D.K.; Zhou, B. Liquid water transport in PEMFC cathode with symmetrical biomimetic flow field design based on Murray's law. *Int. J. Hydrogen Energy* **2021**, *46*, 21059–21074.
179. Tüber, K.; Oedegaard, A.; Hermann, M.; Hebling, C. Investigation of fractal flow-fields in portable proton exchange membrane and direct methanol fuel cells. *J. Power Sources* **2004**, *131*, 175–181. [CrossRef]
180. Cho, J.I.S.; Marquis, J.; Trogadas, P.; Neville, T.P.; Brett, D.J.L.; Coppens, M.O. Optimizing the architecture of lung-inspired fuel cells. *Chem. Eng. Sci.* **2020**, *215*, 115375. [CrossRef]
181. Trogadas, P.; Cho, J.I.S.; Neville, T.P.; Marquis, J.; Wu, B.; Brett, D.J.L.; Coppens, M.O. A lung-inspired approach to scalable and robust fuel cell design. *Energy Environ. Sci.* **2018**, *11*, 136–143.
182. Cho, J.I.S.; Neville, T.P.; Trogadas, P.; Meyer, Q.; Wu, Y.; Ziesche, R.; Boillat, P.; Cochet, M.; Manzi-Orezzoli, V.; Shearing, P.; et al. Visualization of liquid water in a lung-inspired flow-field based polymer electrolyte membrane fuel cell via neutron radiography. *Energy* **2019**, *170*, 14–21.
183. Bethapudi, V.S.; Hack, J.; Trogadas, P.; Hinds, G.; Shearing, P.R.; Brett, D.J.L.; Coppens, M.O. Hydration state diagnosis in fractal flow-field based polymer electrolyte membrane fuel cells using acoustic emission analysis. *Energy Convers. Manag.* **2020**, *220*, 113083. [CrossRef]
184. Iranzo, A.; Arredondo, C.H.; Kannan, A.M.; Rosa, F. Biomimetic flow fields for proton exchange membrane fuel cells: A review of design trends. *Energy* **2020**, *190*, 116435. [CrossRef]
185. Roshandel, R.; Arbabi, F.; Moghaddam, G.K. Simulation of an innovative flow-field design based on a bio inspired pattern for PEM fuel cells. *Renew. Energy* **2012**, *41*, 86–95. [CrossRef]
186. Badduri, S.R.; Srinivasulu, G.N.; Rao, S.S. Influence of bio-inspired flow channel designs on the performance of a PEM fuel cell. *Chin. J. Chem. Eng.* **2020**, *28*, 824–831. [CrossRef]
187. Xie, Q.; Zheng, M. CFD simulation and performance investigation on a novel bionic spider-web-type flow field for PEM fuel cells. *Processes* **2021**, *9*, 1526.
188. Guo, S.; Zhao, Y.; Pan, C.; Wang, X.; Xu, T. Effect of structure parameters on internal mass transfer and performance of PEMFC with spider-web flow field using multi-physical simulation. *Int. J. Hydrogen Energy* **2023**, *48*, 36937–36945.
189. Wang, Z.; Wang, Y.; Yuan, X.; Zhan, H. Design and thermal management of proton exchange membrane fuel cells with biomimetic spider web cooling. *Appl. Therm. Eng.* **2026**, *289*, 129796. [CrossRef]
190. Fan, F.; Tang, S.; Zhang, D.; Fang, H.; Zhang, Y.; Liu, Q. Characterization of high efficiency convective mass transfer for the proton exchange membrane fuel cell: Optimization of the flow field by imitating the spider web morphology. *Int. J. Hydrogen Energy* **2025**, *156*, 150421. [CrossRef]
191. Liu, H.; Tang, X.; Wu, S. Bamboo-inspired flow channels enhance UAV fuel cell performance and economy for agricultural applications. *Int. J. Hydrogen Energy* **2025**, *193*, 152407. [CrossRef]
192. Wang, Y.; Si, C.; Qin, Y.; Wang, X.; Fan, Y.; Gao, Y. Bio-inspired design of an auxiliary fishbone-shaped cathode flow field pattern for polymer electrolyte membrane fuel cells. *Energy Convers. Manag.* **2021**, *227*, 113588.
193. Cai, G.; Liang, Y.; Liu, Z.; Liu, W. Design and optimization of bio-inspired wave-like channel for a PEM fuel cell applying genetic algorithm. *Energy* **2020**, *192*, 116670.
194. Wang, N.; Cheng, Y.; Zhang, L.; Ma, Y.; Fan, X. Performance of proton exchange membrane fuel cell with bionic fish scale porous flow field design. *Energy* **2026**, *344*, 139912. [CrossRef]
195. Zhou, Y.; Miao, Z.; Li, H.; Meng, K.; Chen, B.; Chen, M.; Luo, H.X.; Guan, Y.C.; Duan, Y.X.; Ding, Q.L.; et al. Synergistic multi-physics catalysis enabled by lotus-root-inspired flow fields in proton exchange membrane fuel cells. *J. Mater. Chem. A* **2025**, *13*, 40821–40830.
196. Chen, W.; He, W.; Li, Y.; Zhu, G.; Zuo, Q.; Shen, Z.; Li, J. Fish scale bionic flow field design and performance analysis of a proton exchange membrane fuel cell. *Energy 2025*, 137664.
197. Tanaka, S.; Nagumo, K.; Yamamoto, M.; Chiba, H.; Yoshida, K.; Okano, R. Fuel cell system for Honda CLARITY fuel cell. *eTransportation* **2020**, *3*, 100046. [CrossRef]
198. Hong, B.K.; Kim, S.H.; Kim, C.M. Powering the Future through Hydrogen and Polymer Electrolyte Membrane Fuel Cells: Current commercialisation and key challenges with focus on work at Hyundai. *Johns. Matthey Technol. Rev.* **2020**, *64*, 236–251.

199. Song, Y.; Zhang, C.; Ling, C.Y.; Han, M.; Yong, R.Y.; Sun, D.; Chen, J. Review on current research of materials, fabrication and application for bipolar plate in proton exchange membrane fuel cell. *Int. J. Hydrogen Energy* **2020**, *45*, 29832–29847. [CrossRef]
200. Yoshizumi, T.; Kubo, H.; Okumura, M. *Development of High-Performance FC Stack for the New MIRAI*; SAE Technical Paper; SAE International: Warrendale, PA, USA, 2021.
201. Kim, J.; Luo, G.; Wang, C.Y. Modeling two-phase flow in three-dimensional complex flow-fields of proton exchange membrane fuel cells. *J. Power Sources* **2017**, *365*, 419–429.
202. Zhang, G.; Xie, B.; Bao, Z.; Niu, Z.; Jiao, K. Multi-phase simulation of proton exchange membrane fuel cell with 3D fine mesh flow field. *Int. J. Energy Res.* **2018**, *42*, 4697–4709. [CrossRef]
203. Yu, Z.; Xia, L.; Xu, G.; Wang, C.; Wang, D. Improvement of the three-dimensional fine-mesh flow field of proton exchange membrane fuel cell (PEMFC) using CFD modeling, artificial neural network and genetic algorithm. *Int. J. Hydrogen Energy* **2022**, *47*, 35038–35054.
204. Sun, F.; Su, D.; Li, P.; Dong, X. A novel 3D fine-mesh flow field design and performance analysis for proton exchange membrane fuel cells. *J. Power Sources* **2023**, *584*, 233572. [CrossRef]
205. Sun, F.; Su, D.; Li, P.; Lin, F.; Miu, G.; Wan, Q.; Yin, Y. Effects of three-dimensional type flow fields on mass transfer and performance of proton exchange membrane fuel cell. *Energy* **2024**, *295*, 131111. [CrossRef]
206. Chen, Z.; Ren, W.; Gao, L.; Liu, B.; Pei, S.; Cheng, H.M. Three-dimensional flexible and conductive interconnected graphene networks grown by chemical vapour deposition. *Nat. Mater.* **2011**, *10*, 424–428. [CrossRef] [PubMed]
207. Park, J.E.; Lim, J.; Kim, S.; Choi, I.; Ahn, C.Y.; Hwang, W.; Lim, M.S.; Cho, Y.H.; Sung, Y.E. Enhancement of mass transport in fuel cells using three-dimensional graphene foam as flow field. *Electrochim. Acta* **2018**, *265*, 488–496. [CrossRef]
208. Jang, S.; Park, H.Y.; Jung, J.; Lee, J.; Park, H.Y.; Jang, J.H.; Kim, S.M.; Yoo, S.J. Enhanced water management of three-dimensional graphene-Ni foam with patterned wettability in a polymer electrolyte membrane fuel cell. *ACS Sustain. Chem. Eng.* **2019**, *7*, 15487–15494.
209. Borup, R.L.; Vanderborgh, N.E. Design and testing criteria for bipolar plate materials for PEM fuel cell applications. *MRS Online Proc. Libr.* **1995**, *393*, 151–155. [CrossRef]
210. Zeng, Z.; Yan, C.; Li, Q.; Wang, T. Transport enhancement of proton exchange membrane fuel cell with non-uniform metal foam flow field. *J. Power Sources* **2025**, *657*, 238158. [CrossRef]
211. Lee, N.; Salihi, H.; Yu, B.; Lee, J.; Lee, S.W.; Jang, S.S.; Ju, H. Metal-foam-based cathode flow-field design to improve H2O retention capability of passive air cooled polymer electrolyte fuel cells. *Int. J. Therm. Sci.* **2021**, *161*, 106702.
212. Khatib, F.N.; Wilberforce, T.; Thompson, J.; Olabi, A.G. A comparison on the dynamical performance of a proton exchange membrane fuel cell (PEMFC) with traditional serpentine and an open pore cellular foam material flow channel. *Int. J. Hydrogen Energy* **2021**, *46*, 5984–5998. [CrossRef]
213. Zhang, G.; Bao, Z.; Xie, B.; Wang, Y.; Jiao, K. Three-dimensional multi-phase simulation of PEM fuel cell considering the full morphology of metal foam flow field. *Int. J. Hydrogen Energy* **2021**, *46*, 2978–2989.
214. Ahn, C.Y.; Lim, M.S.; Hwang, W.; Kim, S.; Park, J.E.; Lim, J.; Choi, I.; Cho, Y.H.; Sung, Y.E. Effect of porous metal flow field in polymer electrolyte membrane fuel cell under pressurized condition. *Fuel Cells* **2017**, *17*, 652–661. [CrossRef]
215. Lv, X.; Zhou, Z.; Wu, W.T.; Wei, L.; Gao, L.; Lyu, J.; Li, Y.; Yang, Y.; Li, Y.; Song, Y. Two-phase flow in coupled gas diffusion layer and patterned wettability metal foam flow field in PEM fuel cells. *Renew. Energy* **2025**, *242*, 122419. [CrossRef]
216. Lin, Y.; Sun, Y.; Yang, C.; Zhang, W.; Wang, Q.; Wan, Z.; Ye, C.; Qiu, T. Liquid water discharge capability enhancement of hierarchical pore structure in metal foam flow field of proton exchange membrane fuel cell. *AIChE J.* **2024**, *70*, e18256.
217. Zhang, J.; Huang, H.; Chen, K.; Zhang, R.; Zhang, G.; Wu, W.; Wu, H.; Mo, C.; Mo, J. Effects of gradient porosity in the metal foam flow field on the performance of a proton exchange membrane fuel cell. *Appl. Therm. Eng.* **2024**, *252*, 123638. [CrossRef]
218. Tao, X.; Zeng, Z.; Liu, H.; Suo, M.; Li, Q.; Sun, K.; Che, Z.; Wang, T. PEM fuel cell with non-uniform porous metal foam as cathode flow field. *Appl. Energy* **2025**, *380*, 124938.
219. Sun, Y.; Lin, Y.; Wang, Q.; Yin, W.; Liu, B.; Yang, C.; Wang, Z.; Qiu, T. Design and optimization of bilayer structure in metal foam flow field for proton exchange membrane fuel cell. *Appl. Therm. Eng.* **2024**, *257*, 124305. [CrossRef]
220. Sun, Y.; Lin, Y.; Wan, Z.; Wang, Q.; Yang, C.; Yin, W.; Qiu, T. Water management and performance enhancement in proton exchange membrane fuel cell through metal foam flow field with hierarchical pore structure. *Chem. Eng. J.* **2024**, *494*, 152944. [CrossRef]
221. Li, W.; Zhang, Q.; Wang, C.; Yan, X.; Shen, S.; Xia, G.; Zhu, F.; Zhang, J. Experimental and numerical analysis of a three-dimensional flow field for PEMFCs. *Appl. Energy* **2017**, *195*, 278–288. [CrossRef]
222. Yin, C.; Song, Y.; Liu, M.; Gao, Y.; Li, K.; Qiao, Z.; Tang, H. Investigation of proton exchange membrane fuel cell stack with inversely phased wavy flow field design. *Appl. Energy* **2022**, *305*, 117893. [CrossRef]
223. Gavrailov, D.; Boycheva, S. Comparative Studies of Three-Dimensional Complex Flow Field Designs in a Proton Exchange Membrane Hydrogen Fuel Cell. *Energies* **2025**, *18*, 2165. [CrossRef]

224. Cai, Y.; Fang, Z.; Chen, B.; Yang, T.; Tu, Z. Numerical study on a novel 3D cathode flow field and evaluation criteria for the PEM fuel cell design. *Energy* **2018**, *161*, 28–37. [CrossRef]
225. He, L.; Hou, M.; Gao, Y.; Fang, D.; Wang, P.; Lv, B.; Shao, Z. A novel three-dimensional flow field design and experimental research for proton exchange membrane fuel cells. *Energy Convers. Manag.* **2020**, *205*, 112335. [CrossRef]
226. Sun, Y.; Lin, Y.; Wang, Q.; Yang, C.; Yin, W.; Wan, Z.; Qiu, T. Novel design and numerical investigation of a windward bend flow field for proton exchange membrane fuel cell. *Energy* **2024**, *290*, 130142. [CrossRef]

Disclaimer/Publisher's Note: The statements, opinions and data contained in all publications are solely those of the individual author(s) and contributor(s) and not of MDPI and/or the editor(s). MDPI and/or the editor(s) disclaim responsibility for any injury to people or property resulting from any ideas, methods, instructions or products referred to in the content.